

# **Fabrication and Performance Study of Monolayer Grinding Wheel**

**M.Tech. Thesis**

By  
**Prabhat Kaushik**



**DISCIPLINE OF MECHANICAL ENGINEERING  
INDIAN INSTITUTE OF TECHNOLOGY INDORE**

**JULY, 2018**

# **Fabrication and Performance Study of Monolayer Grinding Wheel**

**A THESIS**

*Submitted in partial fulfillment of the  
requirements for the award of the degree  
of  
Master of Technology*

*by*  
**Prabhat Kaushik**



**DISCIPLINE OF MECHANICAL ENGINEERING  
INDIAN INSTITUTE OF TECHNOLOGY INDORE  
JULY, 2018**



# INDIAN INSTITUTE OF TECHNOLOGY INDORE

## CANDIDATE'S DECLARATION

I hereby certify that the work which is being presented in the thesis entitled **Fabrication and Performance Study of Monolayer Grinding Wheel** in the partial fulfillment of the requirements for the award of the degree of **MASTER OF TECHNOLOGY** and submitted in the **DISCIPLINE OF MECHANICAL ENGINEERING, Indian Institute of Technology Indore**, is an authentic record of my own work carried out during the time period from July, 2016 to July, 2018 under the supervision of Dr. Kazi Sabiruddin, associate professor, Discipline of Mechanical Engineering.

The matter presented in this thesis has not been submitted by me for the award of any other degree of this or any other institute.

**Prabhat Kaushik**

-----  
This is to certify that the above statement made by the candidate is correct to the best of my knowledge.

Signature of the Supervisor

Date:

**Dr. Kazi Sabiruddin**

-----  
**Prabhat Kaushik** has successfully given his M.Tech. Oral Examination held on **13 July 2018**.

Signature of Supervisor of M.Tech. thesis

Date:

Convener, DPGC

Date:

Signature of PSPC Member 1

Date:

Signature of PSPC Member 2

Date:

-----

## ACKNOWLEDGEMENTS

I would like to thank all those people who made this thesis possible and an unforgettable experience for me. This work is a result of the efforts of many individuals, who helped me mentally or physically or both to successfully complete it.

First of all, I would like to express my deepest sense of gratitude to my supervisor Dr. Kazi Sabiruddin, who offered his continued advice and encouragement throughout the course of this thesis. I thank him for the systematic guidance and great effort he put in. I feel greatly privileged to be one of his students.

I am immensely grateful to Dr. Devendra Laxmanrao Deshmukh, Head of Department Mechanical Engineering, for his ever-ready support throughout the work. I acknowledge my gratitude towards Dr. Satyajit Chatterjee and Dr. Sk Safique Ahmad, my PSPC members for their kind suggestions and support during the various presentations of this work.

I am grateful to Sophisticated Instrumentation Centre (SIC), IIT Indore for providing the P-XRD and FESEM facility equipped there. I am thankful to IIT Indore for giving me an opportunity to carry out the research work and providing all the facilities.

I would like to express my very sincere gratitude to Mr. Debjit Misra for the technical assistance to my project to make this thesis possible. His involvement in the work from the first day I joined to the last is highly acknowledged.

I also would like to give my gratitude to the entire batch of M. Tech 2016-2018. I extend my thanks to my flat mates Shivam Goswami and Abhinav Sharma. I am also thankful to my classmates Vivek rana, Ankit Mishra and Arun Ghidode.

Finally, I take this opportunity to express the profound gratitude from my deep heart to my beloved parents and my family for their love and continuous support - both spiritually and materially. The support and love they provide to chase my dream is unmatched.

## **Abstract**

In recent years grinding has gained much significance as a stock removal process, for shaping and sizing both hard and soft materials in contrast to what had been realized in past as the material finishing operation and a process to be worked on very hard materials. In many grinding applications it has become advantageous to use monolayer wheels having grits strongly bonded on a wheel-hub. The bonding layer usually covers 60%-80% of the grit height for effective anchorage of the grits. The successful applications of such wheels have already been reported on grinding at a high speed to achieve high material removal rate. In this study the author has observed that commercially fabricated cBN electroplated wheels may not be free from defects like overplating or growth of galvanic layer in the form of nodules in the space between the grits. Such feature hinders free cutting action and caused wheel loading leading to early termination of wheel life. On the other hand, wheel loading problem has been greatly minimized in a newly developed grinding wheel in which electroplating and electroless plating are used as an interlayer to hold the grits at their respective places while coating with Ni-5Al by using Detonation gun technique. Such type of bond permits to keep the level of the bonding material low but sufficient to hold grits during grinding thus increasing the chip accommodation space. The principal objective of the present work was to investigate the performance of this newly developed wheel with particular reference to its capability to ensure free cutting action by resisting wheel loading.



# CONTENTS

<b>LIST OF FIGURES</b>		<b>v</b>
<b>LIST OF TABLES</b>		<b>ix</b>
<b>ACRONYMS</b>		<b>x</b>
<b>Chapter 1</b>	<b>Introduction</b>	<b>1</b>
<b>1.1</b>	Grinding	<b>1</b>
<b>1.2</b>	Grinding wheel	<b>3</b>
<b>1.3</b>	Single-Layer Wheels	<b>4</b>
<b>1.4</b>	Electroplating	<b>4</b>
<b>1.5</b>	Electroless Plating	<b>5</b>
<b>1.6</b>	Electroplated (Ep) Single-Layer Wheels	<b>6</b>
<b>1.7</b>	Thermal Spray Coating	<b>7</b>
<b>1.7.1</b>	Thermal Spraying	<b>7</b>
<b>1.7.2</b>	Substrate Preparation	<b>8</b>
<b>1.7.3</b>	Coating Material	<b>9</b>
<b>1.7.4.</b>	Detonation-Gun Spraying (D-Gun)	<b>9</b>
<b>1.7.5</b>	Coating Adhesion	<b>10</b>
<b>Chapter 2</b>	<b>Literature Review</b>	<b>12</b>
<b>2.1</b>	Monolayer Grinding Wheels	<b>12</b>
<b>2.2</b>	Detonation Gun	<b>14</b>
<b>Chapter 3</b>	<b>Experimental</b>	<b>15</b>
<b>3.1</b>	Wheel-hub Fabrication	<b>16</b>
<b>3.2</b>	Fabrication of an Adapter to Join Wheel-Hub with Surface Grinder	<b>17</b>
<b>3.3</b>	Wheel-hub Preparation	<b>20</b>

3.3.1	Surface Preparation	20
3.3.2	Grit Blasting	20
3.3.3	Grits Selection	20
3.3.4	Attachment of Grits to Wheel-hub	22
3.4	Electroplating	23
3.5	Electroless Plating	24
3.6	D-Gun Coating	25
3.6.1	D-Gun Coating Analysis	26
3.7	X-ray Diffraction Analysis	26
3.8	Microscopy	27
3.9	Vickers Microhardness Test	27
3.10	Assessment of Substrate Surface Profile	27
3.11	Machining by Fabricated Monolayer Grinding Wheel	27
<b>Chapter 4</b>	<b>Results and Discussions</b>	<b>29</b>
4.1	XRD Study	29
4.1.1	XRD of Al <sub>2</sub> O <sub>3</sub> Grits	29
4.1.2	XRD of Electroless Ni Coating	30
4.1.3	XRD of Ni Electroplated Coating	31
4.1.4	XRD of D-Gun Coated Ni- 5Al	31
4.2	Coating Microstructure Study	32
4.2.1	Electroless Coating	32

<b>4.2.2</b>	Electro-deposition Study	<b>33</b>
<b>4.2.3</b>	D-gun Coating	<b>34</b>
<b>4.3</b>	Coating Hardness Study	<b>36</b>
<b>4.4</b>	Roughness study of coatings	<b>36</b>
<b>4.5</b>	Performance Study of Fabricated Wheels	<b>38</b>
<b>4.5.1</b>	Roughness of workpieces after grinding	<b>42</b>
<b>4.6</b>	Material Removal Rate (MRR) Study	<b>43</b>
<b>4.7</b>	Failure of Grits	<b>45</b>
<b>Chapter 5</b>	<b>Conclusion and Future Scope</b>	<b>49</b>
<b>5.1</b>	Conclusions	<b>49</b>
<b>5.2</b>	Future Scope	<b>50</b>
<b>Chapter 6</b>	<b>Reference</b>	



## LIST OF FIGURES

<b>Figures</b>		<b>Page No.</b>
<b>Fig. 1.1</b>	The six basic elements involved in surface grinding	<b>2</b>
<b>Fig. 1.2</b>	Schematics of monolayer electroplated and brazed CBN wheels	<b>6</b>
<b>Fig. 1.3</b>	Basics mechanism of thermally sprayed coating	<b>8</b>
<b>Fig. 1.4</b>	Schematic of the D-gun process: (1) powder injection; (2) spark plug; (3) gun barrel; (4) oxygen input; (5) nitrogen input	<b>10</b>
<b>Fig. 3.1</b>	Design of the wheel-hubs	<b>16</b>
<b>Fig. 3.2</b>	Image of the wheel-hub after fabrication	<b>17</b>
<b>Fig. 3.3</b>	Design of flange coupling	<b>17</b>
<b>Fig. 3.4</b>	Image of the flange coupling after fabrication	<b>18</b>
<b>Fig. 3.5</b>	Design of the flange made on solidworks	<b>18</b>
<b>Fig. 3.6</b>	Image of the flange after fabrication	<b>19</b>
<b>Fig. 3.7</b>	Image of the final arrangement of the setup after the fabrication	<b>19</b>
<b>Fig. 3.8</b>	FE-SEM image of 16 mesh (1190 $\mu$ m) size Al <sub>2</sub> O <sub>3</sub> grits. Image is of the wheel-hubs after the attachments of grits	<b>21</b>
<b>Fig. 3.9</b>	FE-SEM image of 24 mesh (700 $\mu$ m) size Al <sub>2</sub> O <sub>3</sub> grits	<b>21</b>

<b>Fig. 3.10</b>	FE-SEM image of Al <sub>2</sub> O <sub>3</sub> Grits of 36 (500μm) mesh size	<b>22</b>
<b>Fig. 3.11</b>	Images of the wheel-hubs after the attachment of grits	<b>22</b>
<b>Fig. 3.12</b>	Image of the setup used for Electro-deposition	<b>23</b>
<b>Fig. 3.13</b>	Image of the setup used for electroless deposition	<b>24</b>
<b>Fig. 3.14</b>	Schematic diagram of the coating thickness and the grit coverage	<b>26</b>
<b>Fig. 4.1</b>	X-ray diffraction pattern of alumina grits	<b>29</b>
<b>Fig. 4.2</b>	X-ray diffraction pattern of electroless plated nickel	<b>30</b>
<b>Fig. 4.3</b>	X-ray diffraction pattern of electroplated nickel	<b>31</b>
<b>Fig. 4.4</b>	X-ray diffraction pattern of D-gun coated Ni-5Al	<b>32</b>
<b>Fig. 4.5</b>	Optical microscopy of electroless coated nickel on steel substrate	<b>33</b>
<b>Fig. 4.6</b>	Optical microscopy of electroplated nickel on steel substrate	<b>34</b>
<b>Fig. 4.7</b>	Optical microscopy of D-Gun coated Ni-Al on electroless coated wheel-hub	<b>35</b>
<b>Fig. 4.8</b>	FESEM image of D-Gun coated Ni-5Al on electroless coated	<b>35</b>

	wheel hub	
<b>Fig. 4.9</b>	Micro hardness values of steel substrate, electroplated nickel and electroless coated nickel plating	<b>36</b>
<b>Fig. 4.10</b>	The average Ra values of the different as-deposited coatings.	<b>37</b>
<b>Fig. 4.11</b>	Roughness of the electroplated nickel coating	<b>37</b>
<b>Fig. 4.12</b>	Roughness of the electroless plated nickel coating.	<b>37</b>
<b>Fig 4.13</b>	Roughness of the D-gun coated Ni-5Al on steel substrate	<b>38</b>
<b>Fig 4.14</b>	FESEM image of work piece grinded by the wheel of 16 mesh sized grits	<b>38</b>
<b>Fig 4.15</b>	Image of a chip removed while machining steel workpiece by the wheel of 16-mesh sized wheel.	<b>39</b>
<b>Fig 4.16</b>	FESEM image of workpiece grinded by Grits of 24 mesh size	<b>40</b>
<b>Fig 4.17</b>	Image of chips removed while machining of steel workpiece by 24-mesh sized wheel	<b>40</b>
<b>Fig. 4.18</b>	FESEM image of sample grinded by Grits of 36 mesh size	<b>41</b>
<b>Fig. 4.19</b>	Image of chips removed while machining of steel workpiece by	<b>41</b>

	36-mesh sized wheel	
<b>Fig. 4.20</b>	Comparison graph of Roughness values of surfaces machined using different mesh sized wheels.	<b>43</b>
<b>Fig. 4.21</b>	Material removal rate graph of different types of grinding wheels	<b>45</b>
<b>Fig. 4.22</b>	Comparison of wheels in terms of overall grit failure during machining	<b>46</b>
<b>Fig. 4.23</b>	Percentages of grit pull out and grit breakage for the electroless plated wheels	<b>47</b>
<b>Fig. 4.24</b>	Percentages of grit pull out and grit breakage for the electroplated wheels	<b>48</b>

## LIST OF TABLES

<b>Tables</b>		<b>Page No.</b>
<b>Table 3.1</b>	The grit blasting conditions	<b>19</b>
<b>Table 3.2</b>	Composition of the bath	<b>21</b>
<b>Table 3.3</b>	Bath composition for electroless plating	<b>22</b>
<b>Table 3.4</b>	Used parameters of D-gun sprayed	<b>22</b>
<b>Table 4.1</b>	Average roughness values of the samples	<b>43</b>
<b>Table 4.2</b>	MRR of different grinding wheels	<b>44</b>

## ACRONYMS

<b>cBN</b>	Cubic boron nitride
<b>CVD</b>	Chemical vapour deposition
<b>PVD</b>	Physical vapour deposition
<b>TBC</b>	Thermal barrier coating
<b>SEM</b>	Scanning Electron Microscope
<b>XRD</b>	X ray Diffraction
<b>MRR</b>	Material removal rate



# Chapter 1

## Introduction

### 1.1 Grinding

Grinding is an abrasive material removal and surface generation process used to shape and finish components made of metals and other materials. The precision and surface finish obtained through grinding can be up to ten times better than with either turning or milling. Grinding employs an abrasive product, usually a rotating wheel brought into controlled contact with a work surface. The grinding wheel is composed of abrasive grains held together in a binder. These abrasive grains act as cutting tools, removing tiny chips of material from the work. As these abrasive grains wear and become dull, the added resistance leads to fracture of the grains or weakening of their bond. The dull pieces break away, revealing sharp new grains that continue cutting. The requirements for efficient grinding include [1].

- Abrasive components which are harder than the work
- Shock- and heat-resistant abrasive wheels
- Abrasives that are friable. That is, they are capable of controlled fracturing.

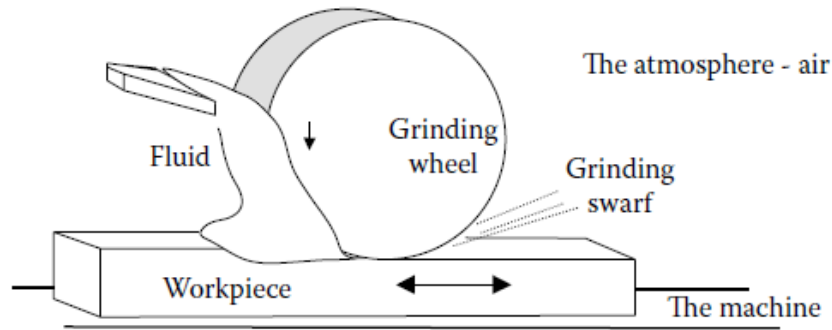


**Fig. 1.1** The six basic elements involved in surface grinding [1].

Most abrasives used in industry are synthetic Aluminum oxide is used in three quarters of all grinding operations, and is primarily used to grind ferrous metals. The next most common manufactured abrasive is ceramic, which is used for grinding hard brittle metals. Ceramic abrasive grains are commonly mixed with aluminum oxide in the manufacture of the wheel to produce better grinding characteristics. Silicon carbide is next, it is used for grinding softer, non-ferrous metals and high density materials, such as cemented carbide or ceramics. Super abrasives, namely cubic boron nitride or ‘cBN’ and diamond, are used in about five percent of grinding. Hard ferrous materials are ground with ‘cBN’, while non-ferrous materials and nonmetals are best ground with diamond. The grain size of abrasive materials is important to the process. Large, coarse grains remove material faster, while smaller grains produce a finer finish. The binders that hold these abrasive grains together include:

- Vitrified bonds, a glass-like bond formed of fused clay or feldspar.
- Organic bonds, from synthetic resins, rubber, or shellac.
- Metal bond, using powder metallurgy or single-layer bond systems.

Wheels are graded according their strength and wear resistance. A ‘hard’ wheel is one that resists the separation of its individual grains. One that is too hard will wear slowly and present dulled grains to the work and overheat, affecting the final finish. If too soft a wheel is used, it will deteriorate quickly, requiring frequent replacement.

Another aspect of grinding wheels is their pore structure or density, which refers to the porosity between individual grains. This pore structure creates spaces between the grains that provide coolant retention and areas for the chips to form. Dense wheels are best for harder materials, while more open densities are better for the softer metals.

The three factors of grain size, bond type, and pore structure are closely related, and together determine how well a wheel will perform [1, 2].

## **1.2 Grinding wheel**

Grinding wheel consists of hard abrasive grains called grits, which perform the material removal through abrasion, held in the weak bonding matrix. A grinding wheel commonly identified by the type of the abrasive material used. The conventional wheels include aluminum oxide and silicon carbide wheels while diamond and cBN (cubic boron nitride) wheels fall in the category of super abrasive wheel.

New abrasives require new ways of working that reflect in new designs of grinding wheel assembly, truing, dressing, and conditioning techniques, coolant delivery and coolant formulation, and finally, new designs of machines capable of high wheel speeds and capable of delivering higher power to the grinding wheel. A variety of wheel designs have developed to cope with differing product geometries.

However, two other considerations gave rise to a new approach to wheel design:

- High wheel speeds must be designed for much greater wheel strength.
- Expensive, but hard-wearing, diamond and cubic boron nitride (cBN) super abrasive only need thin layers of abrasive to achieve a long wheel life.

Modern grinding abrasives mainly fall into one of two groups, namely:-

- Conventional abrasives based either on silicon carbide or aluminum oxide.
- Super abrasives based either on diamond or cubic boron nitride.

The division into two groups is based on a dramatic difference in hardness of the grains leading to very different wheel wear characteristics and grinding strategies. The division is also based on cost; wheels made using super abrasives are typically 10 to 100 times more expensive [2].

### **1.3 Single-Layer Wheels**

Single-layer wheels are generally limited to super abrasives because of the economics of wheel life. They can be subdivided into electroplated wheels fabricated at essentially room temperatures, and brazed wheels fabricated at temperatures as high as 1,000 °C. The following discussion applies in general to plated cubic boron nitrides (cBN) and to plated diamond wheels, although in practice cBN dominates the precision grinding market and is the central focus below [1].

### **1.4 Electroplating**

Nickel electroplating is a commercially important and versatile surface-finishing process. Its commercial importance may be judged from the amount of nickel in the form of metal and salts consumed annually for electroplating, now roughly 100,000 metric tons worldwide, as well as its versatility from its many current applications. The applications of nickel electroplating fall into three main categories: decorative, functional, and electroforming.

There are many functional applications where decoration is not the issue. Instead, nickel and nickel alloys with matte or dull finishes are deposited on surfaces to improve corrosion and wear resistance or modify magnetic and other properties. The properties of nickel electrodeposits produced under different conditions of operation are of particular interest in this connection. Electroforming is electroplating applied to the fabrication of products of various kinds. Nickel is deposited onto a mandrel and then removed from it to create a part made entirely of nickel. A variation of this is electrofabrication where the

deposit is not separated from the substrate and where fabrication may involve electro deposition throughmasks rather than the use of traditional mandrels. The many current applications of nickel electroplating are the result of developments and improvements that have been made almost since the day the process was discovered. This is evident in the following retrospective on the development of nickel electroplating solutions as well as in subsequent sections that deal with basics, decorative electroplating, functional applications and deposit properties, nickel electroforming ,nickel anode materials, quality control, and pollution prevention. Nickel electroplating is similar to other Electrodeposition processes that employ soluble metal anodes; that is, direct current is made to flow between two electrodes immersed in a conductive, aqueous solution of nickel salts. The flow of direct current causes one of the electrodes (the anode) to dissolve and the other electrode (the cathode) to become covered with nickel. The nickel in solution is present in the form positively charged ions. When current flows, the positive ions react with two electrons and are converted to metallic nickel at the cathode surface. The reverse occurs at the anode where metallic nickel is dissolved to form positively charged ions which enter the solution. The nickel ions discharged at the cathode are thus replenished by those formed at the anode [3].

## **1.5 Electroless Plating**

Electroless nickel plating is a process for depositing a nickel alloy from aqueous solutions onto a substrate without the use of electric current. It differs, therefore, from electroplating which depends on an external source of direct current to reduce nickel ions in the electrolyte to nickel metal on the substrate. Electroless nickel plating is a chemical process which reduces nickel ions in solution to nickel metal by chemical reduction. The most common reducing agent used is sodium hypophosphite. Alternatives are sodium borohydride and dimethylamineborane but they are used much less frequently.

Unlike conventional electroplating, no electrical current is required for deposition. The electroless bath provides a deposit that follows all contours of the substrate exactly, without building up at the edges and corners. A sharp edge receives the same thickness of deposit as does a blind hole. The base substrate being plated must be catalytic in nature. A properly prepared workpiece provides a catalyzed surface and, once introduced into the electroless solution, a uniform deposition begins. Minute amounts of the electroless metal (i.e., nickel, copper, etc.) itself will catalyze the reaction, so the deposition is autocatalytic after the original surfaces are coated. Electroless deposition then continues, provided that the metal ion and reducing agent are replenished. If air or evolved gas, however, are trapped in a blind hole or downward facing cavity, this will prevent electroless deposition in these areas. In electroless plating, metal ions are reduced to metal by the action of chemical reducing agents, which are simply electron donors. The metal ions are electron acceptors, which react with electron donors. The catalyst is the workpiece or metallic surface, which accelerates the electroless chemical reaction allowing oxidation of the reducing agent. [5]

## 1.6 Electroplated Single-Layer Wheels

Electroplated wheels consist of a single layer of super abrasive grains bonded to a precision machined steel blank using nickel deposited by an electroplating or occasionally Electroless plating process. The plating depth is controlled to leave about 50% of the abrasive exposed.

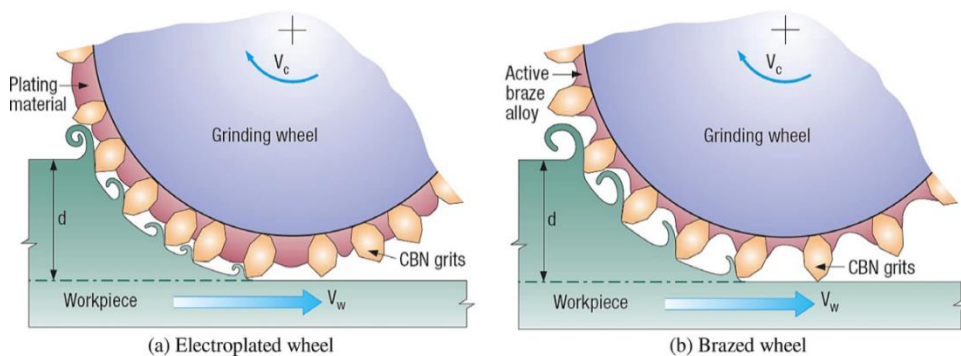


**Fig. 1.2** Schematics of monolayer electroplated and brazed CBN wheels. [4]

## 1.7 Thermal Spray Coating

### 1.7.1 Thermal Spraying

Thermal spray is a generic term for a group of coating processes used to apply metallic or nonmetallic coatings. These processes are grouped into three major categories: flame spray, electric arc spray, and plasma arc spray. These energy sources are used to heat the coating material (in powder, wire or rod form) to a molten or semi-molten state. The resultant heated particles are accelerated and propelled toward a prepared surface by either process gases or atomization jets. Upon impact, a bond forms with the surface, with subsequent particles causing thickness buildup and forming a lamellar structure. The thin “splats” undergo very high cooling rates, typically in excess of  $10^6 \text{ K s}^{-1}$  for metals. A major advantage of thermal spray processes is the extremely wide variety of materials that can be used to produce coatings. Virtually any material that melts without decomposing can be used. A second major advantage is the ability of most thermal spray processes to apply coatings to substrates without significant heat input. Thus, materials with very high melting points, such as tungsten, can be applied to finely machined, fully heat-treated parts without changing the properties of the part and without excessive thermal distortion of the part. A third advantage is ability, in most cases, to strip off and recoat worn or damaged coatings without changing part properties or dimensions. A disadvantage is the line-of-sight nature of these deposition processes. They can only coat what the torch or gun can “see.” It is impossible to coat small, deep cavities into which a torch or gun will not fit. Thermal spraying can provide thick coatings (approx. thickness range is 20 micrometers to several mm, depending on the process and feedstock), over a large area at high deposition rate as compared to other coating processes such as electroplating, CVD and PVD [6].

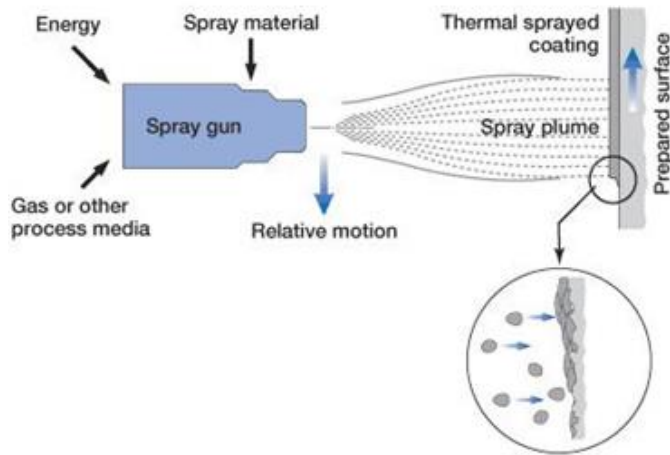


**Fig. 1.3** Basics mechanism of thermally sprayed coating [6]

Coating materials available for thermal spraying include metals, alloys, ceramics, plastics and composites. They are fed in powder or wire form, heated to a molten or semi - molten state and accelerated towards substrates in the form of micrometer-size particles. Combustion or electrical arc discharge is usually used as the source of energy for thermal spraying. Resulting coatings are made by the accumulation of numerous sprayed particles. The surface may not heat up significantly, allowing the coating of flammable substances [5].

### 1.7.2 Substrate Preparation

The adhesion of the coating to the substrate predominantly consists of mechanical bonding, careful cleaning and pretreatment of the surface to be coated is extremely important. After the removal of surface impurities by chemical or mechanical methods, the surface is usually roughened using a blasting procedure. The liquid or molten coating particles impact the surface at high speed. Heat from the hot particles is transferred to the cooler base material. As the particles shrink and solidify, they bond to the roughened base material. Adhesion of the coating is therefore based on mechanical “locking”.

The amount of metallurgical bond caused by diffusion between the coating particles and the base material is small and can be neglected for discussions about bonding mechanisms. Surface roughening usually takes place via grit blasting with dry corundum. In addition, other media, such as chilled iron, steel grit or SiC are used for some applications. Besides the type of grit, other important factors include particle size, particle shape, blast angle, pressure and purity of the grit media [7].

### **1.7.3 Coating Material**

In principle, any material that does not decompose as it is melted can be used as a thermal spray coating material. Depending on the thermal spray process, the coating material can be in wire or powder form. Choosing a coating material that is suitable for a specific application requires special knowledge about the service environment as well as knowledge about the materials. Apart from the physical characteristics, such as coefficient of expansion, density, heat conductivity and melting point, additional factors, such as particle shape, particle size distribution and manufacturing process of powder material (i.e. sintered, composited) will influence coating performance [7].

### **1.7.4 Detonation-Gun Spraying (D-Gun)**

The D-gun, shown schematically in Figure 1.4, includes a long, water-cooled barrel with an ID of about 25mm.

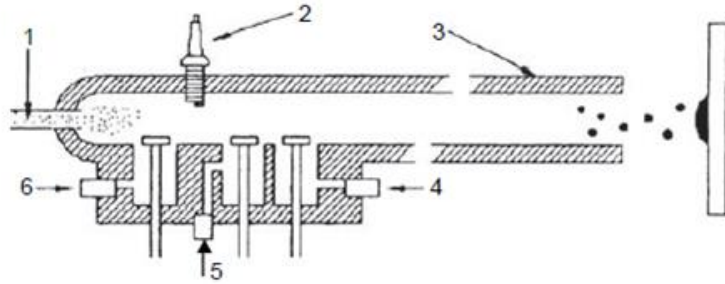


**Fig.1.4** Schematic of the D-gun process: (1) powder injection; (2) spark plug; (3) gun barrel; (4) oxygen input; (5) nitrogen input. [8]

A mixture of oxygen (4) and acetylene (5) is fed into the barrel, together with a charge of powder (1). The gas is ignited, explodes and its detonation wave accelerates the powder. In order to avoid ‘backfiring’, i.e. explosion of the fuel gas supply, an inert gas, such as nitrogen, is used between the portions of exploding mixture. Nitrogen also purges the barrel. The detonation process therefore has the following cycles:

- Injection of oxygen and fuel into the combustion chamber;
- Injection of powder and nitrogen to prevent ‘backfiring’;
- Ignition of mixture and acceleration of powder;
- Purging of barrel by nitrogen.

There are 1–15 detonations per second with purges of nitrogen between them [8].

### 1.7.5 Coating Adhesion

Adhesion is the tendency of dissimilar particles or surfaces to hold tightly to one another. It is viewed as the strength of the bonds between the coating material and the substrate. Coating adhesion is the "condition in which two surfaces are held together by either

valence forces or by mechanical anchoring or by both together“. The coating should well adhere to the substrate so that it can function properly without spall off and tolerate the mechanical and thermal stresses.

Mechanical, chemical and metallurgical factors may contribute to the adhesion of the coating to the substrate. The adhesion strength of hard ceramic coating on a steel substrate also simultaneously depends on

1. The substrate surface texture.
2. The value of surface average roughness (Ra).

The two surfaces may have the same value of average roughness but a non-identical surface texture which may show a different behavior for adhesion strength of coating on a substrate. The deposition of thermally sprayed hard ceramic coating on the steel substrate is always problematic due to the difference in the thermal expansion coefficient and contraction of the steel substrate and hard ceramic coating may cause the shearing of the coating at the interface. The possible solutions to overcome are

1. To have proper metallurgical compatibility an intermediate layer between the substrate and the coating (called as Bond Coat) can be applied. The thermal property of bond coat is in between the top layer and the substrate.
2. By improving the mechanical interlocking between the substrate and the coating

## Chapter 2

### Literature Review

#### 2.1 Monolayer Grinding Wheels

**Chattopadhyay et al.** studied that the surface of a cup shaped galvanically bonded CBN grinding wheel showed undesirable growth of the bonding layer in the form of nodules in the space between the grits. This was true for both blocky type and microcrystalline type CBN grits. With such a working surface, the advantage of a galvanically bonded wheel was drastically offset. Nodule formation not only reduced the chip accommodation space but also led to intensified bond-chip, bond-work interaction thus increasing grinding force, spindle power and temperature. Galvanically bonded monolayer CBN wheels even with coarse grit (B 251) failed to work efficiently with a depth of cut of 30 microns while grinding unhardened 100 Cr6 steel under the wet condition because of the loading problem. Further investigation is necessary to analyze the causes of nodule formation on the surface of a cup shaped galvanically bonded monolayer CBN wheel. It is particularly important because of the fact that none of the wheels fabricated by several manufacturers was absolutely free from such imperfection [9].

**Chattopadhyay et al.** studied that in the newly developed grinding wheel bonding of chemical nature permitted use of low thickness of the bonding layer to hold the grits on a steel disc while having sufficient adhesion between the grit and bonding material. The wheel with coarser grits offered very stable grinding action while grinding both GG40 cast iron and unhardened 100Cr6 steel without any noticeable increase in normal force and spindle power. No wheel loading was observed when ductile steel was ground even at high infeed under dry condition. During grinding with wheel having finer grit size (B126), brittle material like cast iron did not cause any chip storage problem at any infeed

value. The situation was entirely different when 100Cr6 steel was ground with wheel having finer grits. Within a short time loading started at relatively low infeed value [10].

**Chattopadhyay and Hintermann** studied that high crystal exposure which happens to be the essence of the brazed bonded diamond tools, could not always be maintained in the commercially manufactured tools because of accumulation of bonding material in the space between the grits. Thus, in some discrete places on the wheel face the effective grit protrusion was much reduced. Irregular grit distribution as well as non-uniform layer thickness of the braze alloy were found to throw strong influence on the formation of an uneven brazed bond on the monolayer abrasive tool surface after brazing. The uniformity of grit protrusion could be improved by regular grit distribution and maintaining uniform layer thickness of the braze alloy. The improvement in crystal exposure did not make any noticeable difference in the performance of two types of wheels when grinding oxide ceramic. The grinding behavior of both wheels changed markedly because of rapid grit wear. The selection of appropriate type of diamond which can provide high wear resistance is of immense importance in such applications [11].

**Chattopadhyay and Hintermann** studied that In comparison to a galvanically bonded single layer cBN tool, brazed bonded counterparts have strong grit-bond adhesion. Performance of a brazed cBN wheel could be remarkably improved by placing the grains in a regular manner [12].

**Palet al.** studied that when compared to the galvanically bonded wheel, the brazed-type wheel showed better performance in grinding of the bearing steel. The brazed-type wheel could grind the bearing steel more effectively and economically with lesser grinding forces and without wheel loading over wide ranges of the grinding parameters. The main characteristics of the brazed-type wheel behind its better performance mainly are higher bond strength, larger grit protrusion and more control on uniformity of grits' spacing on

the wheel surface. The relative benefits of using the brazed-type wheel over the galvanically bonded wheel increased with the increase in MRR and volume of material removal [13].

**Bhaduri and Chattopadhyay** studied that TiN coated wheel could not perform better than the uncoated wheel during grinding of low carbon steel due to high wheel loading. However, the uncoated wheel was found to undergo fracture wear, which was remarkably absent in the coated wheel. The situation was totally different during grinding of hardened bearing steel, where benefit of TiN coating within a particular range of substrate bias was clearly revealed. The uncoated wheel was found to undergo many fracture wear with some pull-out of grits. On the other hand, almost no pull-out and much less fractured grits were observed in the wheels coated at bias voltages like -60 V and -90 V. However, neither a very low (like 0 V) nor a too high bias (like -120 V and -150 V) was found to arrest the grit fracture at bond level [14].

## 2.2 Detonation Gun

**Wang et al.** studied that thermal barrier coating are extensively in hot section components in gas turbine, engines for jet aircraft and power generator. Two types of thermal shock testing were adopted. Firstly, the specimens were exposed to air at 1050 °C for 10 minutes and forced air cooling to room temperature. Second, thermal cycling consisted of directly inserting samples to 1100 °C holding for 10 minutes and then water quenching. Results show that the D gun coating with lamellar structure had a low thermal conductivity as compared to plasma sprayed YSZ coating and much lower than EB- PVD due to microstructure difference. TBC obtained by D gun spraying with a few micro cracks in ceramic coat and a rough bond coat surface exhibited excellent resistance to thermal shock up to 400 cycles for 1<sup>st</sup> shock test and 200 cycles for 2<sup>nd</sup> shock test [15].

**Wang and Liu** studied that the residual stresses has significant effect on the coating performance, such as adhesive strength, resistance to thermal shock, erosion resistance. To investigate the effect of residual stress on adhesive behavior, the adhesion of WC-Co coatings with different thickness against corresponding residual stress is plotted. It is seen that the adhesion of compressively stressed coatings was better than that of the coatings with tensile stress. So the results show that the larger compressive residual stress can result in a stronger adhesion between the coating and substrate [16].

**Sumith** studied that the hardness of alumina+40% Ti is increased more when compared to uncoated Aluminium and alumina oxide. SEM images show increased abrasion resistance in alumina+40% Ti as compared to uncoated aluminum and alumina oxide. Corrosion resistance is highest in alumina+40% Ti [17].

## Chapter 3

## Experimental

### 3.1 Wheel-hub fabrication

Steel substrates are used for this experiment; AISI 1020 steel substrates are considered for fabrication of the wheelhub. The substrates are grit blasted inside a suction type grit blasting cabinet using alumina grits of 24 mesh size, pressure of 100 psi and with a standoff distance of 100 mm. The grit blasted samples are cleaned ultrasonically. The wheel-hubs are fabricated on lathe. Figure 3.1 shows the design of the wheel-hubs. Fig. 3.2 shows the wheelhub after fabrication.

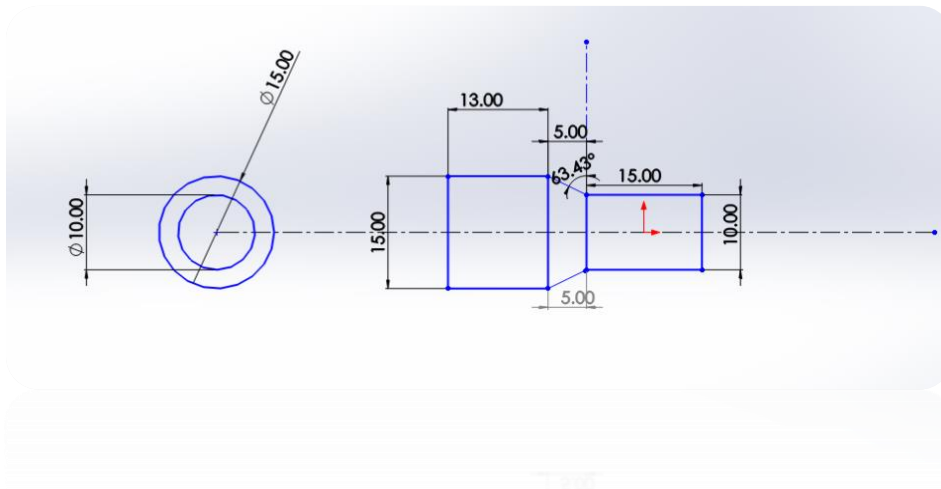


**Fig. 3.1** Design of the wheel-hubs



**Fig. 3.2** Image of the wheel-hub after fabrication

### **3.2 Fabrication of an adapter to join Wheel-hub with Surface Grinder**

AISI 1020 steel has been considered for fabrication of the adapter. The flange coupling adapter is fabricated on lathe. The design of the setup is done on solidworks. Figure 3.3- figure 3.7 show the design of flange coupling and the final arrangement of the setup.

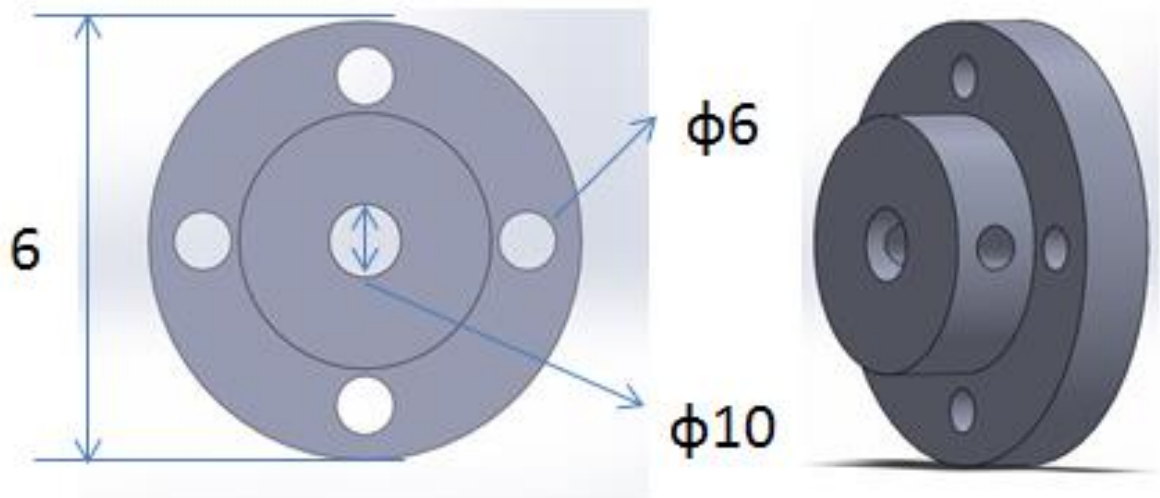


**Fig. 3.3** Design of flange coupling



**Fig. 3.4** Image of the flange coupling after fabrication

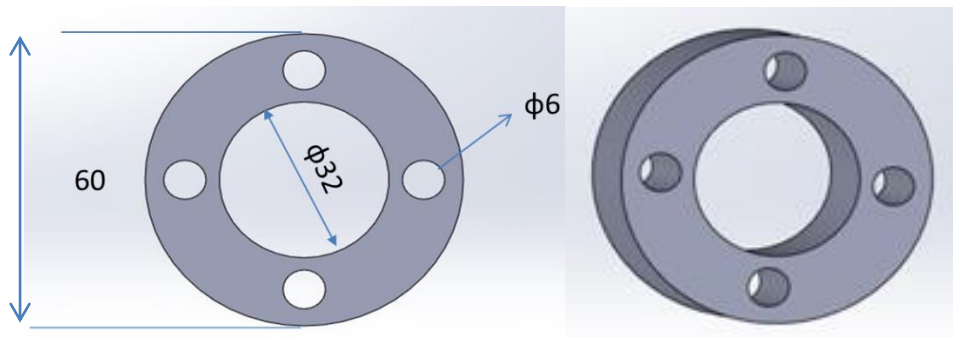


**Fig. 3.5** Design of the flange made on solidworks



**Fig. 3.6** Image of the flange after fabrication

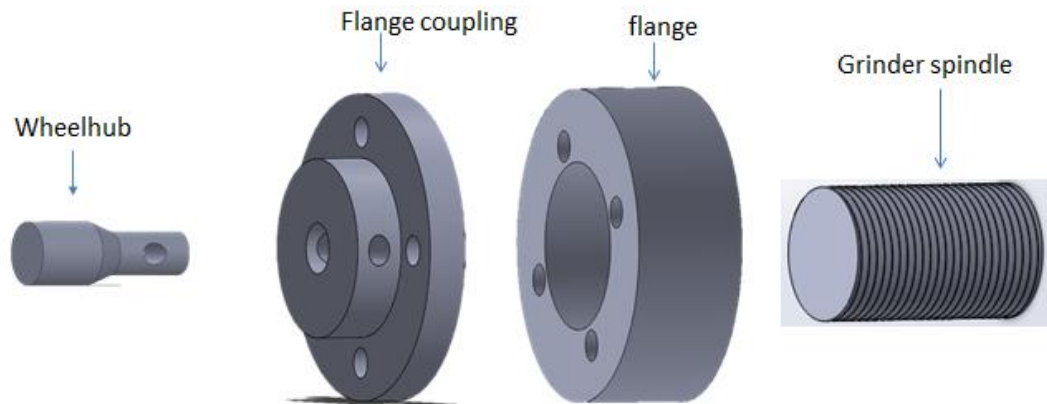


**Fig. 3.7** Image of the final arrangement of the setup after the fabrication

### 3.3 Wheel-hub preparation

#### 3.3.1 Surface preparation

Surface preparation is an essential first stage treatment of a substrate before the application of any type of coating. Purposes of surface preparation prior to the coating are:-

1. Removal of scale, oil, grease, and paint.
2. Improvement of adhesion of coating with substrate through mechanical interlocking.

#### 3.3.2 Grit blasting

In grit blasting technique, dry abrasive particles are propelled towards the substrate at relatively high speed. Alumina grits are used for roughness generation.

The grit blasting conditions are as follows (Table 3.1)

**Table 3.1:** The grit blasting conditions

<b>Substrate</b>	<b>Number of substrate analyzed</b>	<b>Grit type &amp; size</b>	<b>Blasting pressure (bar)</b>	<b>Standoff distance (mm)</b>	<b>Blasting angle (degree)</b>	<b>Blasting time (sec.)</b>
Carbon steel (AISI 1020)	9	Alumina, 16 grits	4	100	90	60

#### 3.3.3 Grit selection

Al<sub>2</sub>O<sub>3</sub> grit is known for its hardness and strength. It is widely used as an abrasive material for grit blasting. In addition to this, it is much less expensive substitute for industrial diamond/cBN. Al<sub>2</sub>O<sub>3</sub> grits of 16 mesh(1190μm), 24 mesh (700μm), and 36 mesh

(500 $\mu\text{m}$ ) are used in this study. Figure 3.8 – figure 3.10 show the SEM images of the  $\text{Al}_2\text{O}_3$  grits. All the grits are crushed type with sharp edges.

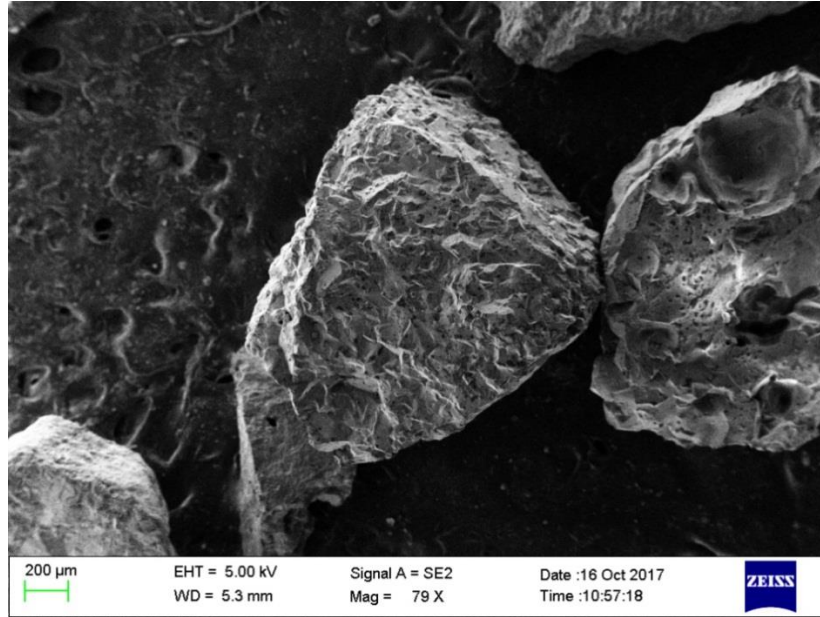


**Fig. 3.8** FE-SEM image of 16 mesh (1190 $\mu\text{m}$ ) size  $\text{Al}_2\text{O}_3$  grits.

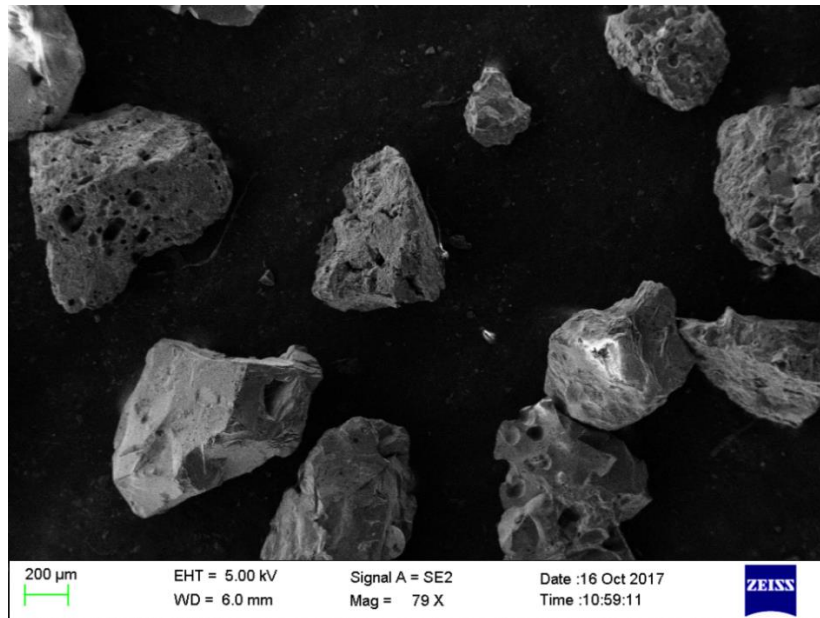


**Fig. 3.9** FE-SEM image of 24 mesh (700 $\mu\text{m}$ ) size  $\text{Al}_2\text{O}_3$  grits.

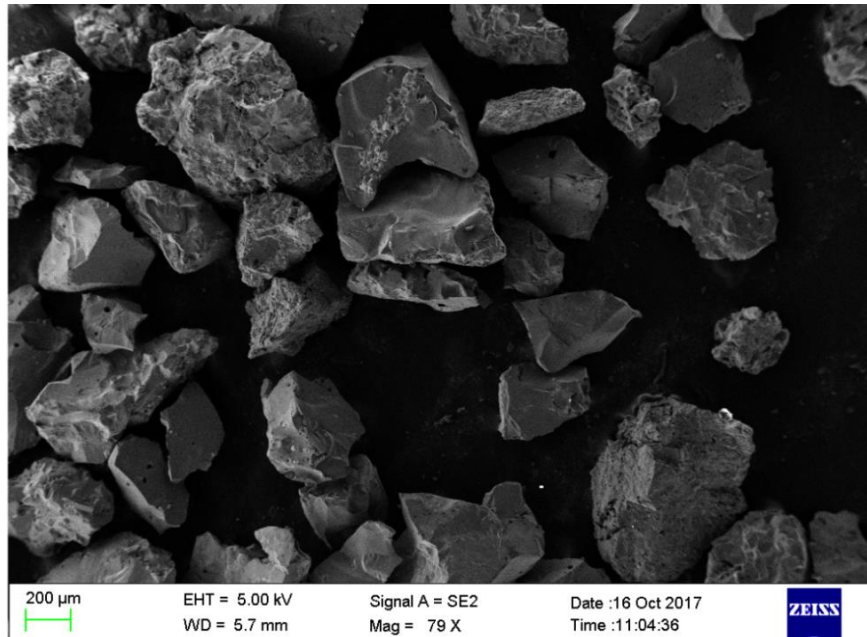


**Fig. 3.10** FE-SEM image of  $\text{Al}_2\text{O}_3$  Grits of 36 (500 $\mu\text{m}$ ) mesh size

### 3.3.4 Attachment of grits to wheel-hub

Grits are attached to the wheel-hub using epoxy resin (araldite). The grit spacing is decided as per the literature for standard monolayer wheels. Figure 3.8 shows the image of the wheel-hubs after the attachment of grits:-

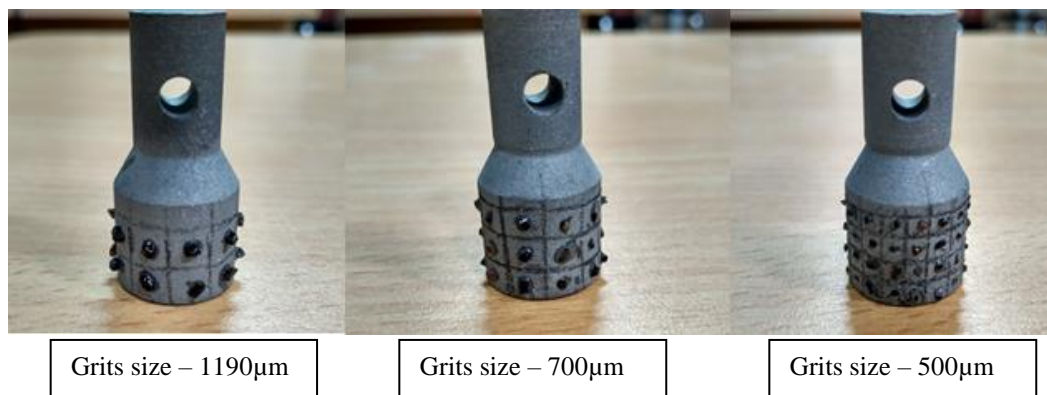


**Fig. 3.11** Images of the wheel-hubs after the attachment of grits

### 3.4 Electroplating

The wheels are Ni electroplated using Electrodeposition technique. Figure 3.9 shows the setup used for Electrodeposition and table 3.2 shows the composition of the bath used for Electrodeposition. By controlling the process parameters a Ni base coating with a thickness of around 100 $\mu$ m is deposited on grit attached wheel-hub.

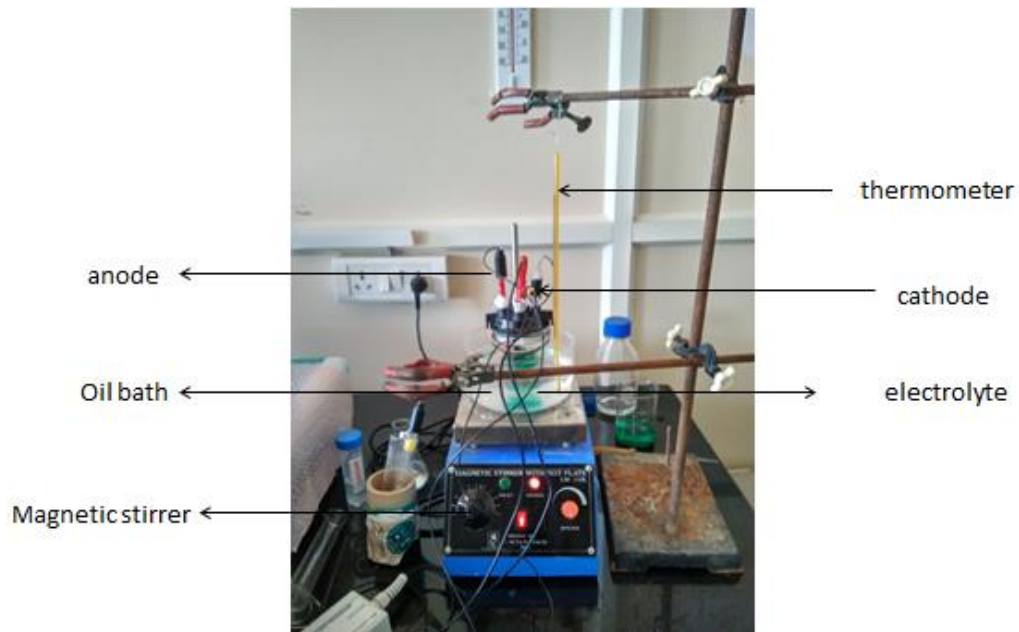


**Fig. 3.12** Image of the setup used for Electro-deposition

**Table 3.2:** Composition of the bath

Nickel sulfate ( $\text{NiSO}_4$ )	180 g/L
Ammonium chloride( $\text{NH}_4\text{Cl}$ )	25 g/L
Boric acid( $\text{H}_3\text{BO}_3$ )	30 g/L
pH	5.6 - 5.9
Temperature	43 - 60 $^\circ\text{C}$

### 3.5 Electroless Plating

The prepared wheel-hubs are electroless plated with nickel (Ni). Figure 3.10 shows the setup used for electroless deposition and table 3.3 shows the bath composition for electroless deposition. By controlling the process parameters Ni is deposited on the grit attached wheel-hubs with a thickness of around  $50\mu\text{m}$ .

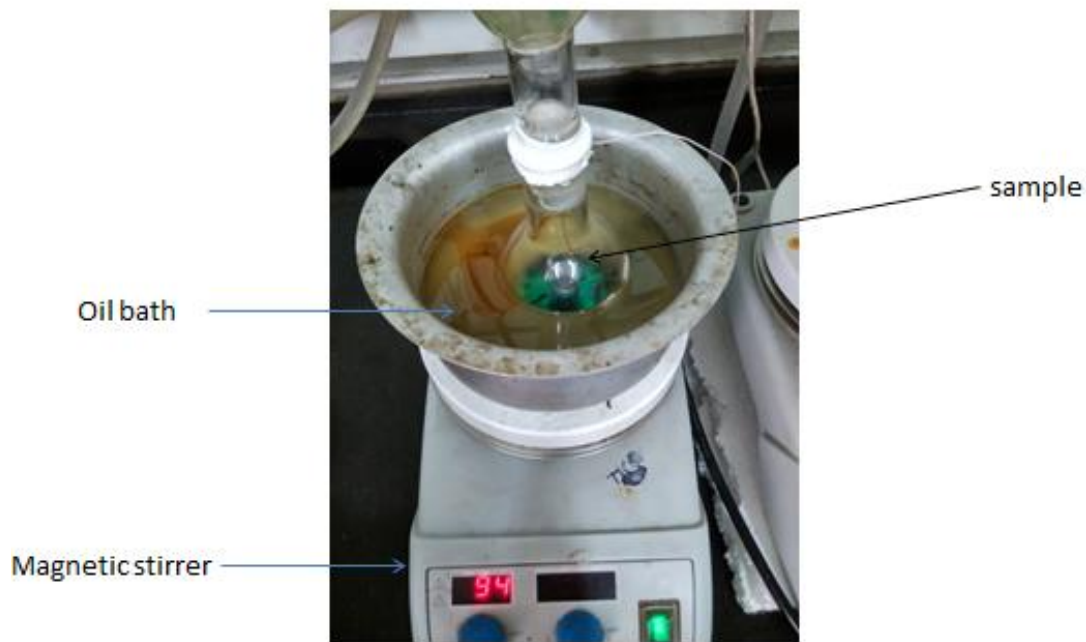


**Fig. 3.13** Image of the setup used for electroless deposition

**Table 3.3:** Bath composition for electroless plating

Nickel sulfate (NiSO <sub>4</sub> )	33 g/L
Sodium citrate(Na <sub>3</sub> C <sub>6</sub> H <sub>5</sub> O <sub>7</sub> )	84 g/L
Ammonium chloride(NH <sub>4</sub> Cl)	50 g/L
Sodium hypophosphite(NaPO <sub>2</sub> H <sub>2</sub> )	17 g/L
pH	8-9
Temperature	85 °C

### 3.6 D-Gun Coating

Ni-5Al powder is successively deposited over the electroplated and electroless plated substrates by detonation gun process(D-Gun) [SVX private ltd., Awaaz Detonation gun].Table 3.4 shows the used process parameter for D-Gun coating technique. A Ni-5Al coating with a thickness of 60 µm is deposited on the electroplated and electroless plated wheel-hubs.

**Table 3.4:** Used parameters of D-gun sprayed

Parameters	Value
Firing rate (Hz)	1-10
Number of shot per second	5
Coating thickness per shot (µm)	5-25
Relative humidity of ambient air (%)	50

### 3.6.1 D-Gun coating analysis

Figure 4.14 shows the schematic diagram of the coating thickness of the electroless/electroplated coating and the detonation gun coating on the wheel-hub surface and the grit coverage.

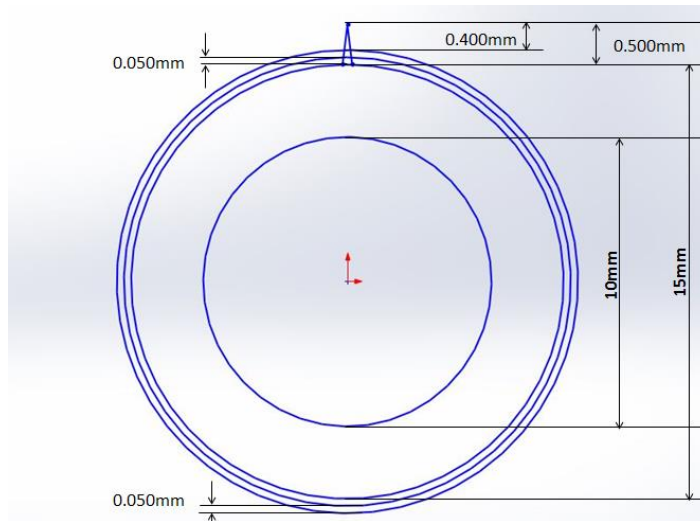


**Figure 3.14** Schematic diagram of the coating thickness and the grit coverage

### 3.7 X-ray Diffraction Analysis

The phases of the coatings are identified by using X-ray diffraction method. X-ray diffraction (XRD) analyses of the coated surfaces are done by using an X-ray diffractometer (*Rigaku Smart Lab 3 kW*) with nickel-filtered Cu K $\alpha$  radiation ( $\lambda=0.15406$  nm) operating at 30 kV and 40 mA. X ray is generated using a copper target, operated at 30 kV and 40 mA. The data is collected from 20° angle to 100° angle with a step size of 0.01° and a counting time of 1s per step.

### **3.8 Microscopy**

The coating cross-section is polished with standard polishing technique. The polished samples are observed under optical microscope (Leica, DFC 295) and scanning electron microscope (FESEM, Zeiss Supra-55) to study the coating microstructure.

### **3.9 Vicker's Microhardness Test**

The hardness of the coatings is measured by using a UHL-002 microhardness tester with a load of 25gf and dwell time of 15s. An average of minimum 10 readings for each sample is considered.

### **3.10 Assessment of substrate surface profile**

The roughness of the substrates and the as deposited coatings are assessed by contact type stylus profilometer (Taylor-Hobson, Surtronic 25). The average surface roughness (Ra) and the 2D profile of the rough surface is obtained.

### **3.11 Machining by fabricated monolayer grinding wheel**

Using the fabricated grinding wheels the steel (AISI 1020) plates (20 mm×10mm×10mm) are grinded in surface grinder (BJ-9140T). The MRR (material removal rate, mm<sup>3</sup>/min) for each wheel is estimated by calculating material removal and the duration of machining. The number of grits damaged by different modes is also calculated. Further,

the MRR of fabricated wheels are compared with the same of standard  $\text{Al}_2\text{O}_3$  wheel used for surface finish.

## Chapter 4

## Result and Discussion

### 4.1 XRD study

#### 4.1.1 XRD of Al<sub>2</sub>O<sub>3</sub> grits:-

X-ray diffraction pattern of Al<sub>2</sub>O<sub>3</sub> grits is shown in figure 4.1. These grits are produced by crushing and grinding to have a chunky morphology. The irregular shapes of the grits are shown in figure 3.8- figure 3.10. All different alumina grits reveal the peaks of  $\alpha$ -Al<sub>2</sub>O<sub>3</sub> phase only. Being hardest in nature these  $\alpha$ -Al<sub>2</sub>O<sub>3</sub> phase has higher disintegration property compared to the other phases of Al<sub>2</sub>O<sub>3</sub>.

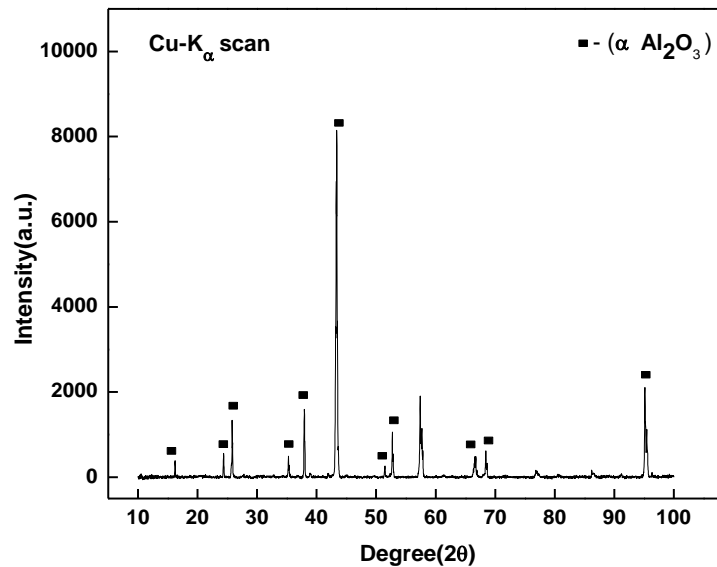


**Fig. 4.1** X-ray diffraction pattern of alumina grits

### 4.1.2 XRD of Electroless Ni Coating

In figure 4.2 the XRD pattern of electroless Ni coating show the presence of Ni (OH)<sub>2</sub> in the coating. As electroless coating is slow and a self-catalytic coating process, the incoming Ni ions towards the anode substrate forms Ni(OH)<sub>2</sub> by combining with (OH)<sup>-</sup> ions and deposit over the wheel-hub. This coating has good coverage of the surface and anchors the grits strongly with the cylindrical surface of the wheel-hub. However, as the Ni<sup>++</sup> ions form compound on the substrate, the adhesion of the coating material might not be as strong as the pure Ni deposits.

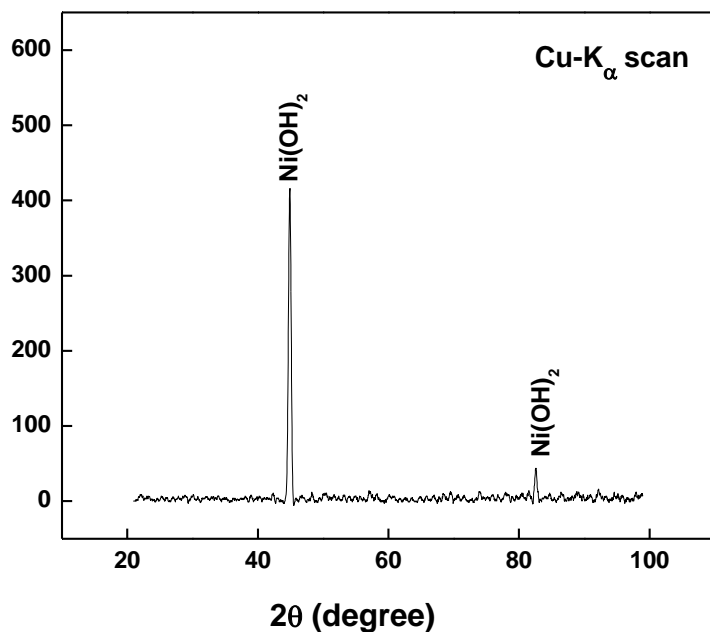


**Fig. 4.2** X-ray diffraction pattern of electroless plated nickel

### 4.1.3 XRD of Ni Electroplated Coating

In figure 4.3 the XRD pattern of electroplated Ni coating shows the major presence of Ni in the coating. Along with Ni peaks few peaks of Ni(OH)<sub>2</sub> are also observed. The coating coverage is good and provides a good amount of adhesion to the Al<sub>2</sub>O<sub>3</sub> grits.

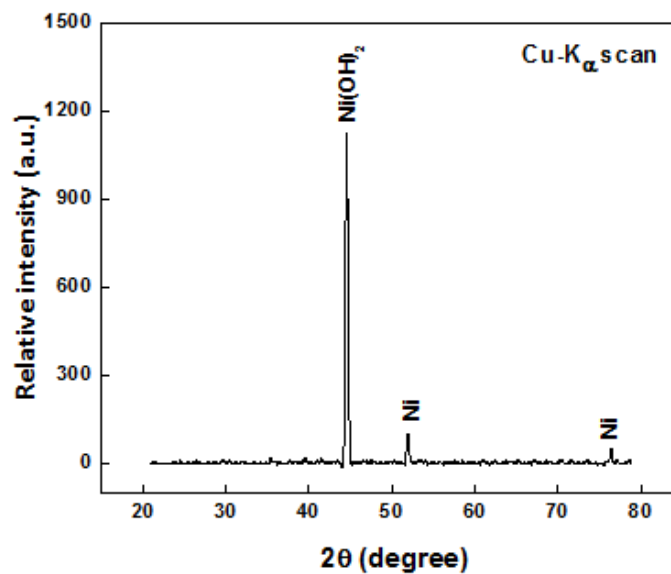
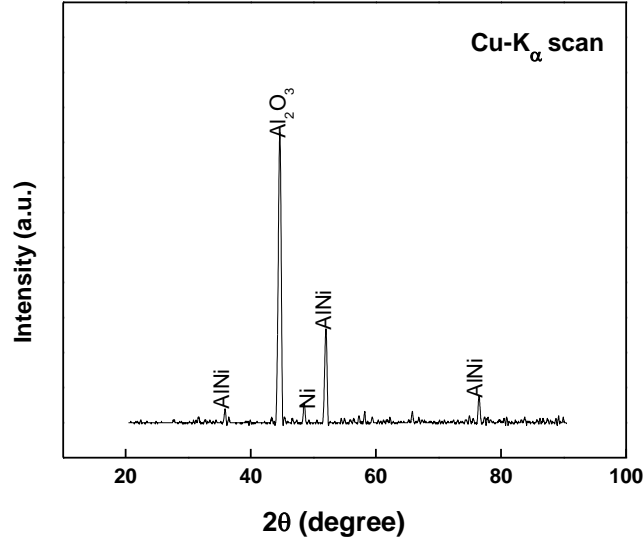


Fig. 4.3 X-ray diffraction pattern of electroplated nickel

### 4.1.4 XRD of D-Gun coated Ni-5Al

In figure 4.4 the XRD pattern of D-gun coated nickel reveals the presence of Ni-Al alloy, Ni and Al<sub>2</sub>O<sub>3</sub> in the coating. The presence of Al<sub>2</sub>O<sub>3</sub> is due to the grits attached to the wheel-hub.



**Fig. 4.4** X-ray diffraction pattern of D-gun coated Ni-5Al

## 4.2 Coating Microstructure Study

### 4.2.1 Electroless coating

Four samples are nickel plated using electroless deposition technique. The nickel coating is expected to hold the grits at their respective positions during the detonation gun coating process. Thickness of the coating is kept between 40-50 microns. In figure 4.5, the image of coating microstructure captured by optical microscope is shown. The porosity seems to be less and the adhesion of the coating with the substrate seems to be satisfactory.

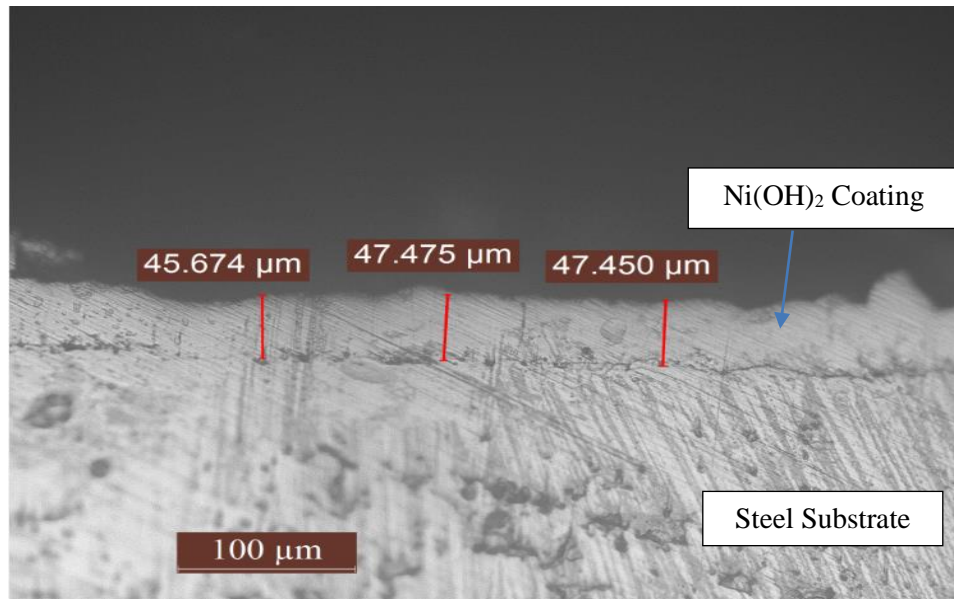


**Fig. 4.5** Optical microscopy of electroless coated nickel on steel substrate

#### **4.2.2 Electro-deposition study**

Five samples are nickel plated by using Electroplating technique. The nickel coating is expected to hold the grits at their respective positions during the detonation gun coating process. The thickness of the coating is kept between 110-130 microns. In figure 4.6, the coating microstructure is shown. The porosity of the coating seems to be very less with strong adhesion with the steel substrate.

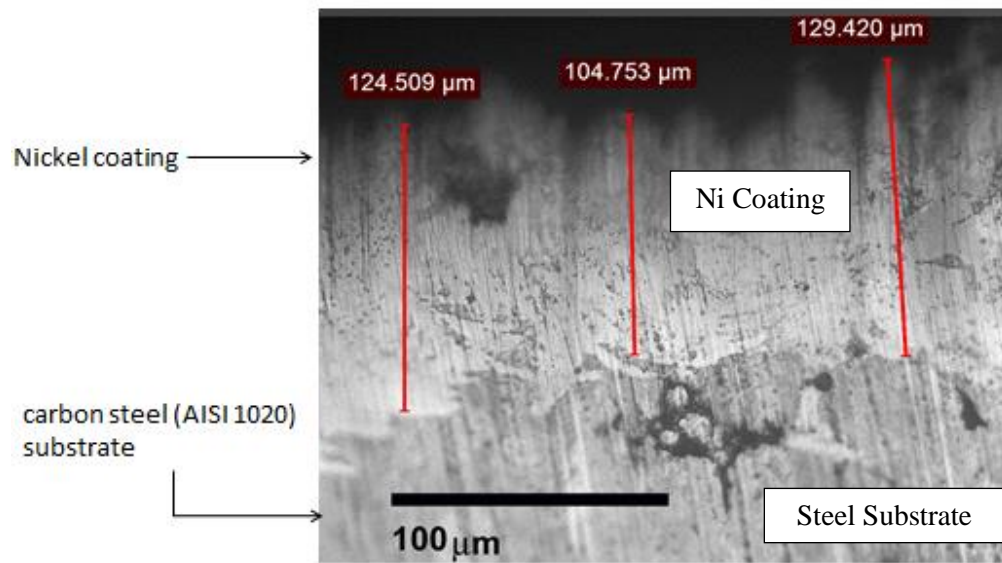


**Fig. 4.6** Optical microscopy of electroplated nickel on steel substrate

### 4.2.3 D-gun coating

Figure 4.7 and figure 4.8 show the micrographs of D-gun coated Ni-Al deposited on the electroless plated sample. The D-Gun coating is porous in nature and like a typical thermally sprayed coating. In some locations the adhesion of D-gun coating (Ni-5Al) seems to be good with no gap at the interface. However, the overall mismatch of Ni-5Al coating with electroless Ni(OH)<sub>2</sub> with high gap is observed. This is due to the formation of H<sub>2</sub>O vapour during the application of D-gun coating at high temperature which causes dissociation of Ni(OH)<sub>2</sub> into Ni and H<sub>2</sub>O. This H<sub>2</sub>O vapour causes separation between the two coatings. So the adhesion seems to be weak.

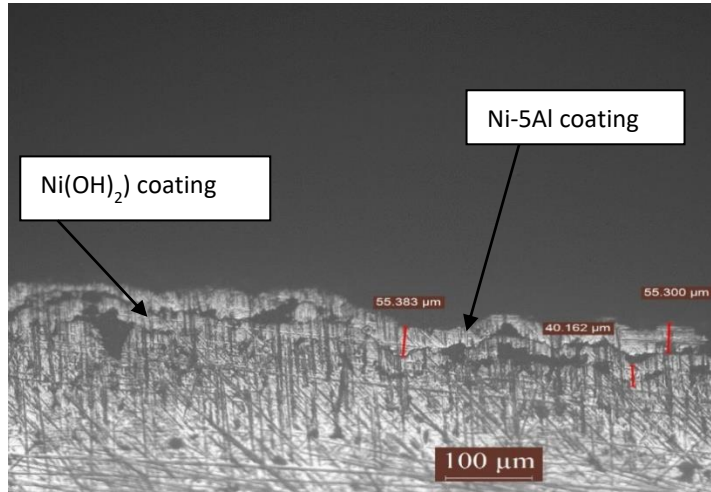


**Fig. 4.7** Optical microscopy of D-Gun coated Ni-Al on electroless coated wheel-hub

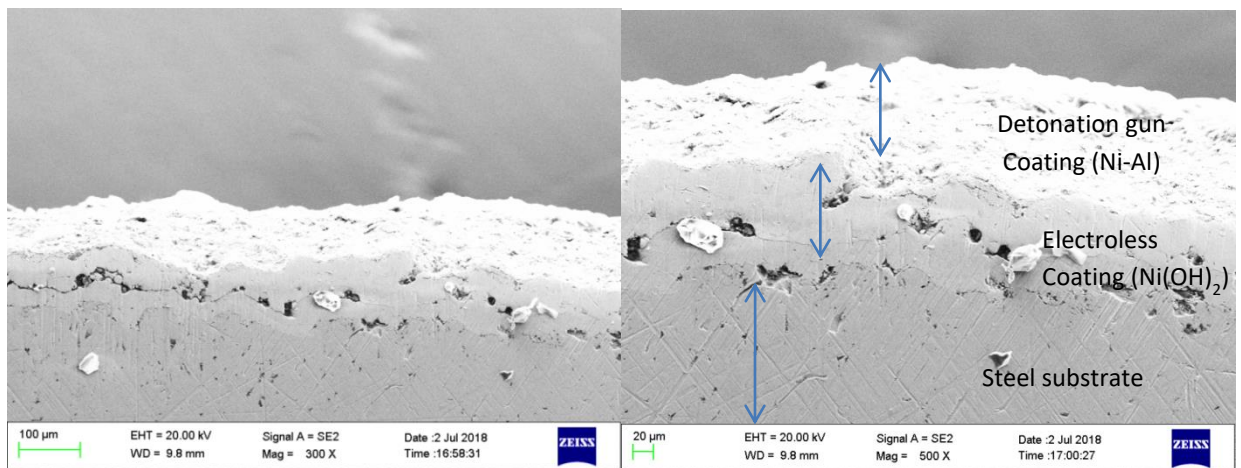


**Fig. 4.8** FESEM image of D-Gun coated Ni-5Al on electroless coated wheel hub

### 4.3 Coating Hardness Study

The Vickers hardness test result shown in figure 4.9 suggests that the hardness of electroplated Ni coating is much lower than the same of electroless Ni coating. This is due the presence of internal stress of electroplated coating which reduces the hardness of a material. On the other hand due to low internal stress of coating material the hardness of electroless Ni coating is more.

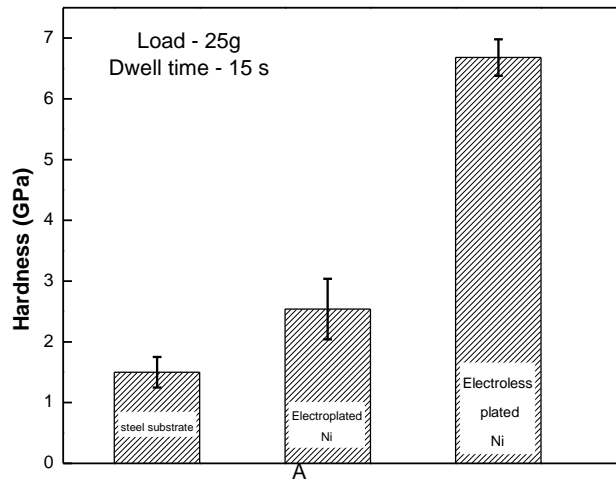


**Fig. 4.9** Micro hardness values of steel substrate, electroplated nickel and electroless coated nickel

### 4.4 Roughness study of coatings

In figure 4.10 the average Ra values of the different as-deposited coatings are shown. Due to the ionic deposition in case of electroplated and electroless coatings the Ra values are very less. Whereas due to the splat deposition, the Ra value of the D-gun coating is

remarkably high. Apparently, the roughness of electroplated/electroless coated Ni helps the D-gun coated material to achieve proper adhesion through mechanical interlocking. Figure 4.11 – figure 4.13 show the roughness profiles of the coatings from electroplating, electroless plating and detonation gun respectively.

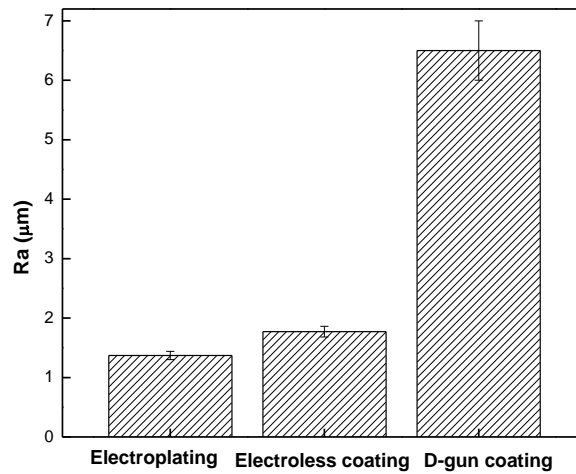


**Fig 4.10** The average Ra values of the different as-deposited coatings.

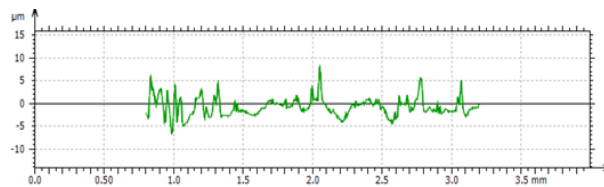


**Fig 4.11** Roughness of the electroplated nickel coating

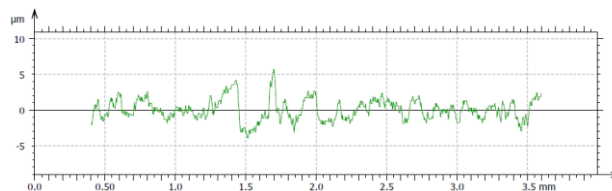


**Fig 4.12** Roughness of the electroless plated nickel coating

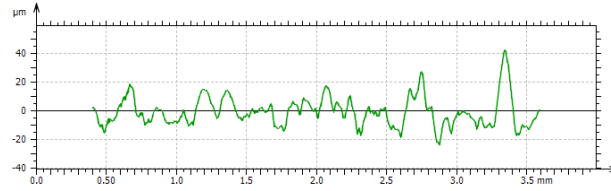


**Fig 4.13** Roughness of the D-gun coated Ni-5Al coating

## 4.5 Performance Study of Fabricated Wheels

In figure 4.14 the machined surface of steel workpiece by wheel of 16-mesh is shown. It shows severe damage of the surface. The width of the crater created by the grits is large. Severe burr formation is also noticed on the surface. These burrs are still attached to the ductile surface. Longer chips are also observed during machining. Figure 4.15 shows the image of a chip removed while machining the steel workpiece by using wheel with grits of 16-mesh size.

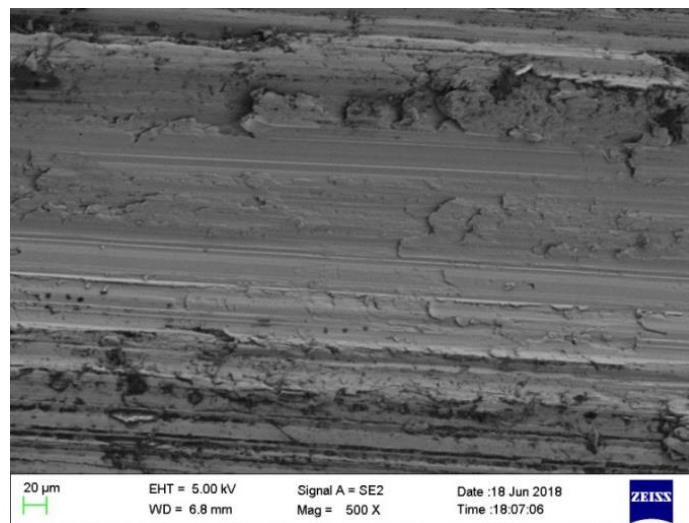


**Fig. 4.14** FESEM image of work piece grinded by the wheel of 16 mesh sized grits

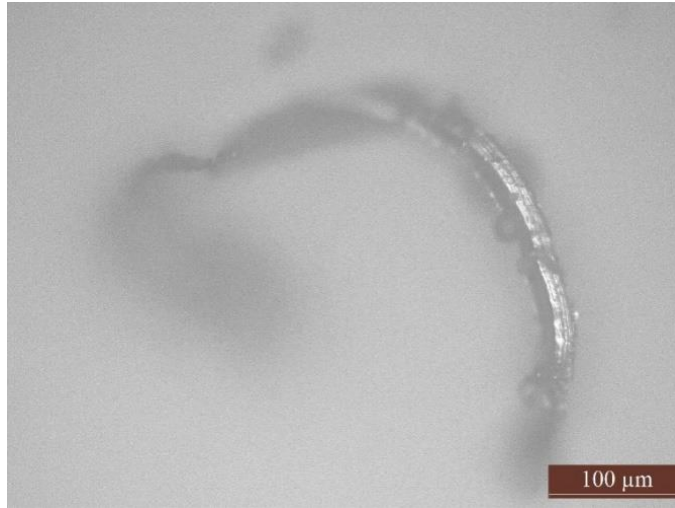


**Fig 4.15** Image of a chip removed while machining steel workpiece by the wheel of 16-mesh sized wheel.

In figure 4.16 the machined surface of steel by the wheel of 24-mesh sized grit is shown. It shows the damaged surface with small burrs attached to it. The width of the lay is relatively smaller than the same produced by 16-mesh sized wheel. During machining, both small and large chips are observed. Figure 4.17 shows the image of chips after grinding the workpiece with 24-mesh sized wheel.

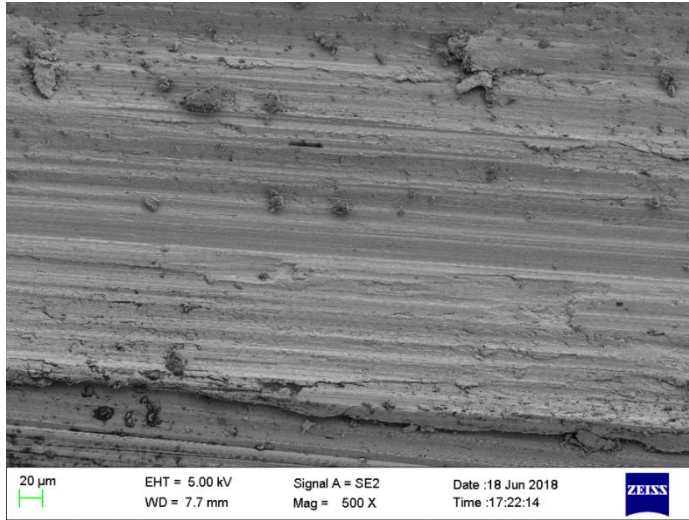


**Fig. 4.16** FESEM image of workpiece grinded by Grits of 24 mesh size

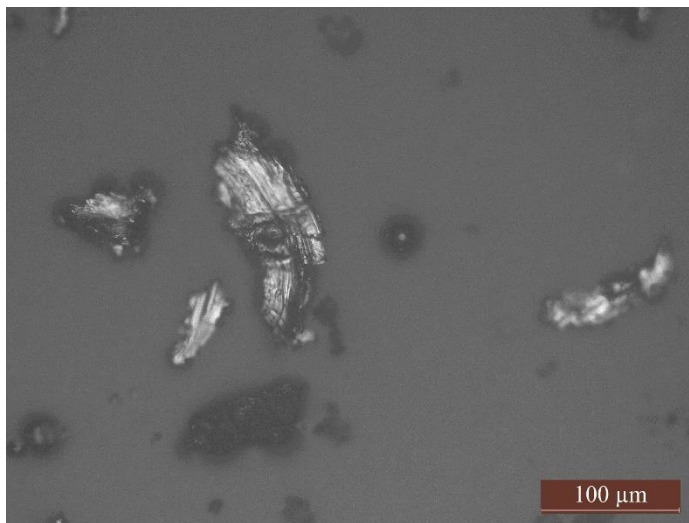


**Fig. 4.17** Image of chips removed while machining of steel workpiece by 24-mesh sized wheel

In figure 4.18 the machined surface of the steel workpiece by the wheel of 36-mesh sized grits is shown. The lay produced by the machining process have much lower depth in it. The width of the lay is very small and smaller chips are formed. Few small chips or burrs

are found to be attached to the surface. Figure 4.19 shows the chips after grinding the workpiece with 36-mesh sized wheels.

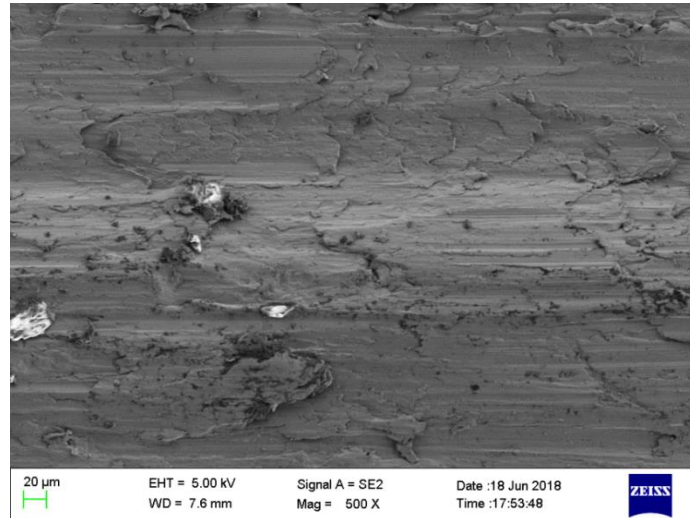


**Fig. 4.18** FESEM image of sample grinded by Grits of 36 mesh size

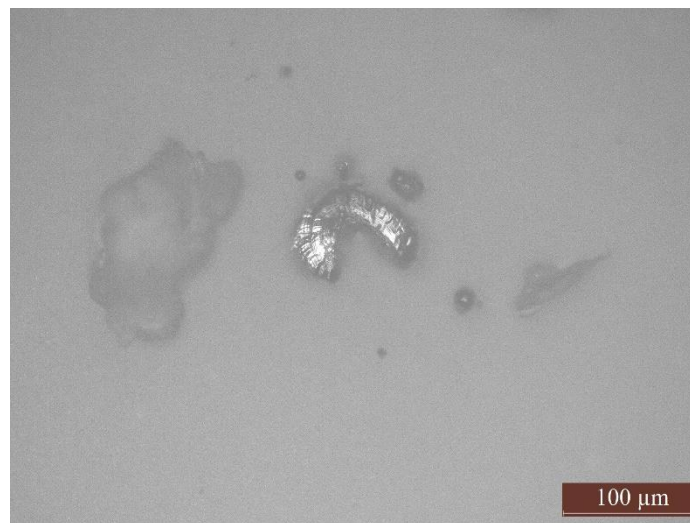


**Fig 4.19** Image of chips removed while machining of steel workpiece by 36-mesh sized wheel

#### 4.5.1 Roughness of machined surfaces

Table 4.1 depicts the average roughness (Ra) values of machined surfaces after grinding by using wheels of different grit sizes. Larger grits produce rougher surfaces than the smaller grits. Figure 4.20 illustrates the comparison of surfaces in terms of roughness values. This suggests that for good surface finish, wheel of smaller grits can be used and for high material removal wheel with larger grits can be used.

**Table 4.1** Average roughness values of the samples

Wheel (mesh size)	Sample no.	Ra value	Average Ra
16 mesh	Sample 1	6.08	6.13333
16 mesh	Sample 2	6.22	
16 mesh	Sample 3	6.10	
24 mesh	Sample 4	5.23	5.21667
24 mesh	Sample 5	5.18	
24 mesh	Sample 6	5.24	
36 mesh	Sample 7	5.01	5.01333
36 mesh	Sample 8	4.94	
36 mesh	Sample 9	5.09	
Conventional wheel	Sample 10	4.23	--

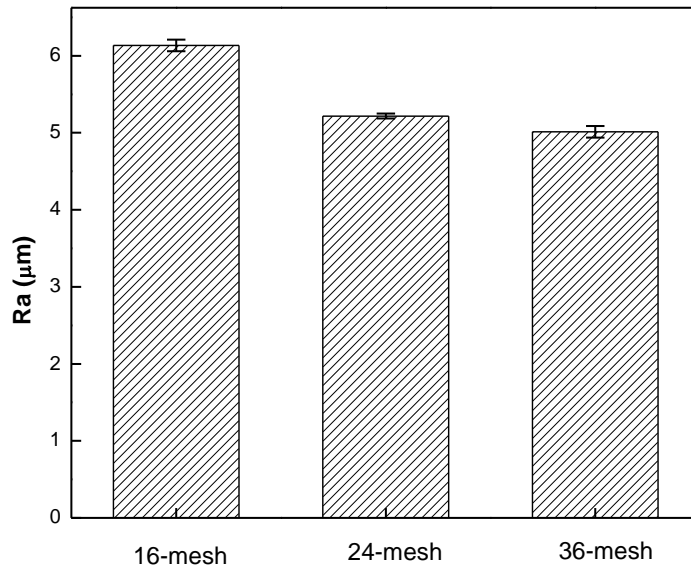


**Fig 4.20** Comparison graph of Roughness values of surfaces machined using different mesh sized wheels.

#### 4.6 Material removal rate (MRR) study

The calculated material removal rates of different tools for different technologies and grit sizes are shown in table 4.2. The corresponding data is shown in figure 4.21 by a bar chart. In figure 4.20, it is noticed that with an increase in mesh size (decreasing particle size) the MRR value decreases. The MRR values obtained from wheels of 16-mesh and 24-mesh sized grits are higher than the same of conventional wheel. The MRR obtained from electroplated wheel is very close to MRR value obtained by conventional wheel in case of 36-mesh sized grits. It is also observed that for any grit size, the MRR of electroplated wheel is always more than the same of electroless coated wheel. This is due to the presence of  $\text{Ni(OH)}_2$  in electroless coating. This  $\text{Ni(OH)}_2$  probably forms water vapour at high temperature applications such as D-Gun coating and grinding. At such

high temperatures the tool becomes weaker by forming H<sub>2</sub>O vapour at the interface of electroless coating and D-Gun coating.

**Table 4.2** MRR of different grinding wheels

<b>Wheel type</b>	<b>Sample no.</b>	<b>MRR (mm<sup>3</sup>/min.)</b>	<b>Coating type</b>
16 mesh	Sample 1	61.8	Electroplating
16 mesh	Sample 2	58.44	Electroplating
16 mesh	Sample 3	47.64	Electroless
24 mesh	Sample 4	37.14	Electroplating
24 mesh	Sample 5	32.4	Electroless
24 mesh	Sample 6	31.14	Electroless
36 mesh	Sample 7	24.12	Electroplating
36 mesh	Sample 8	15.10	Electroplating
36 mesh	Sample 9	12.86	Electroless
Conventional wheel	Sample 10	23.76	-

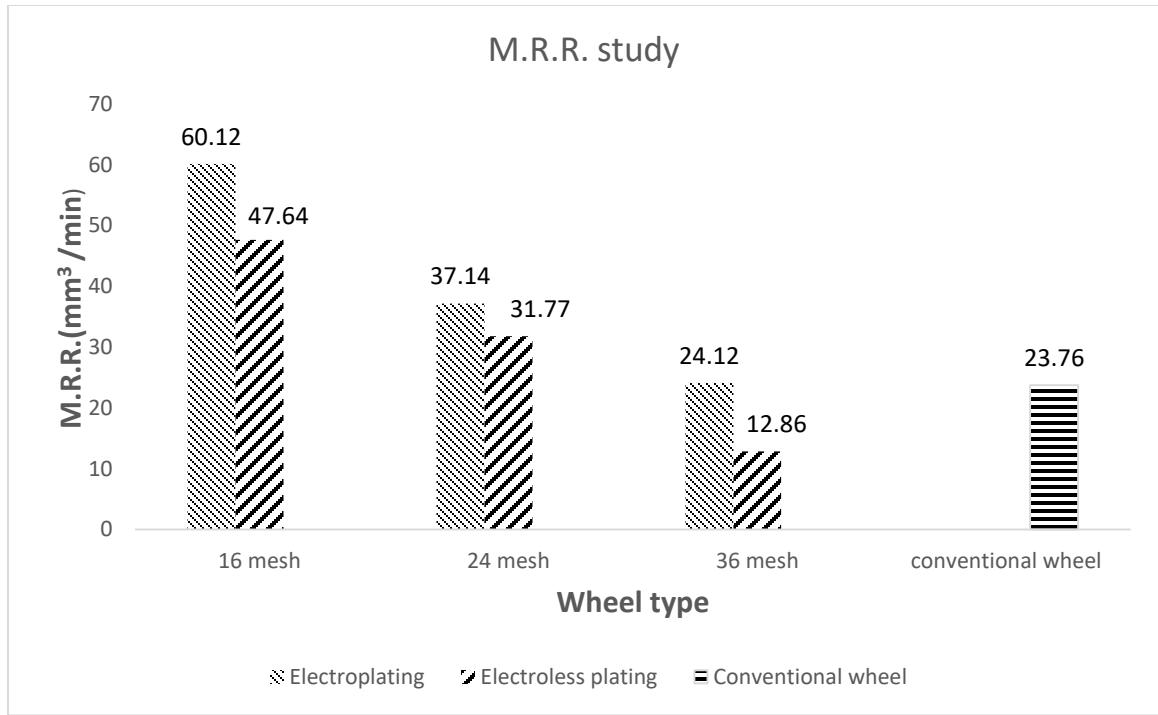


**Fig. 4.21** Material removal rates of different grinding wheels

#### 4.7 Failure of Grits

In figure 4.22 the percentage failure of grits during machining are shown for different wheels. Failure of grits is more in case of electroless coated wheels compared to the same of electroplated wheels. This is due to the weak adhesion of the grits in case of electroless coated wheels. The change in percentage of grit damage is not significant in case of electroplated wheels with changing mesh size. However, for electroless coated wheels significant change in grit failure with changing mesh size is observed. The maximum grit failure is observed for wheels with 24-mesh sized grits.

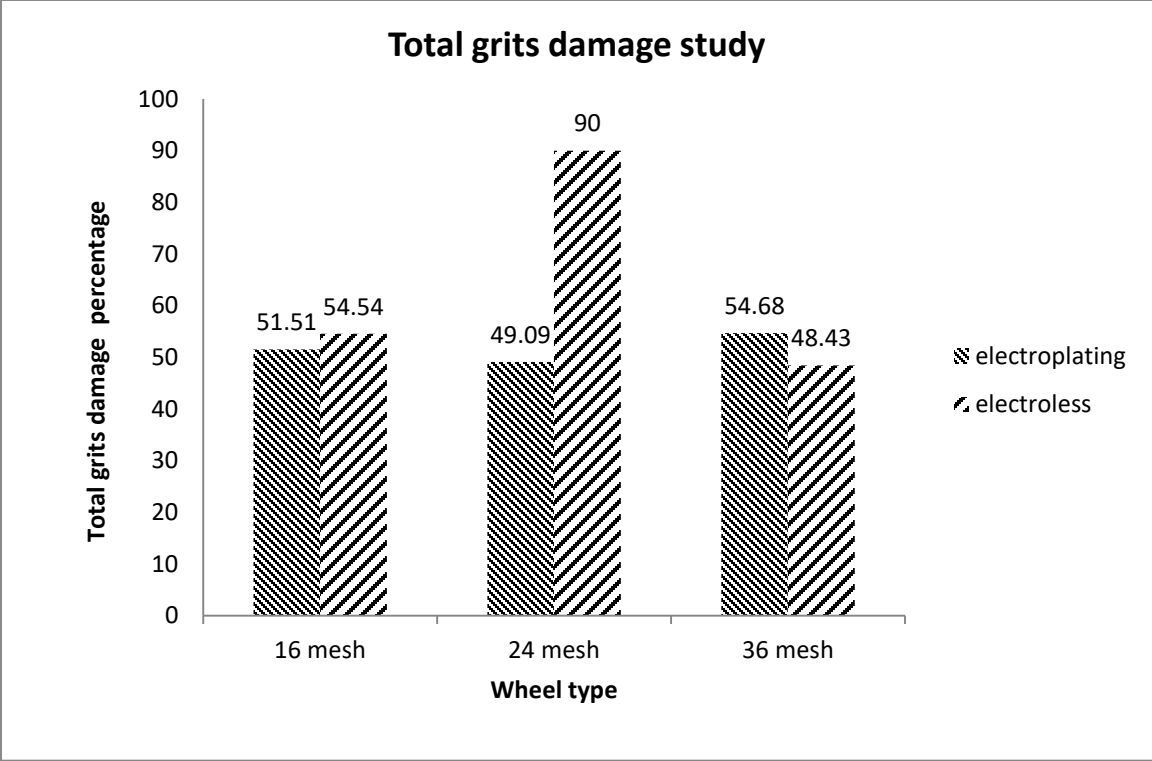


**Fig. 4.22** Comparison of wheels in terms of overall grit failure during machining

In figure 4.23 the grit pull-out and grit breakage percentages for electroless coated wheels are shown graphically. It shows for any grit size, the pull-out numbers are significantly higher than the grit breakage numbers. It suggests the weak adhesion of grits with the wheel-hub. Grit pull out is maximum in case of wheel of 24 mesh sized grits.

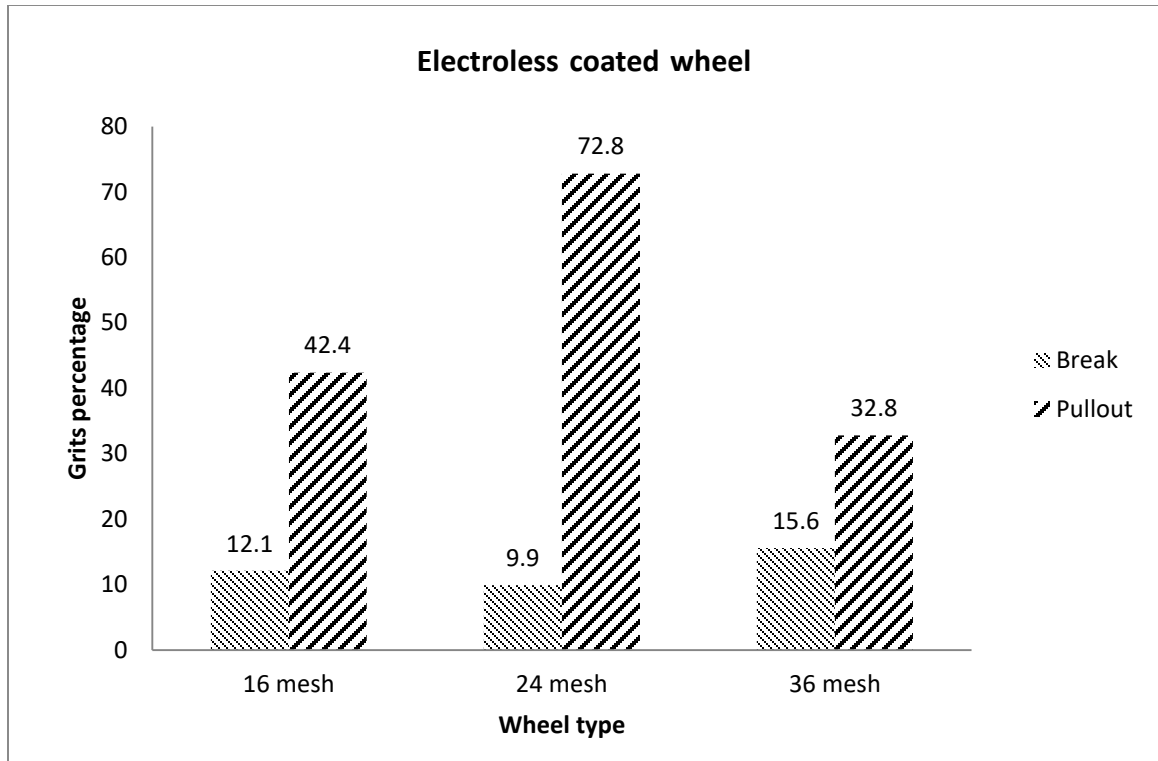


**Fig. 4.23** Percentages of grit pull out and grit breakage for the electroless plated wheels

In figure 4.24 the percentages of grit breakage and grit pull-out for electroplated wheels are shown graphically. It shows the grit pull-out numbers are less compared to the grit breakage number for 16-mesh and 24-mesh sized grits. With an increase in mesh size the breakage number decreases. This is due to the change in uncoated portion of grits which experiences the tangential force and the individual grit acts like a cantilever. More is the length of the uncoated portion; more is the chance of breakage. On the other hand, with an increase in mesh size the grit pull-out number increases. However, these values are not as high as the values obtained in the case of electroless coated wheels.

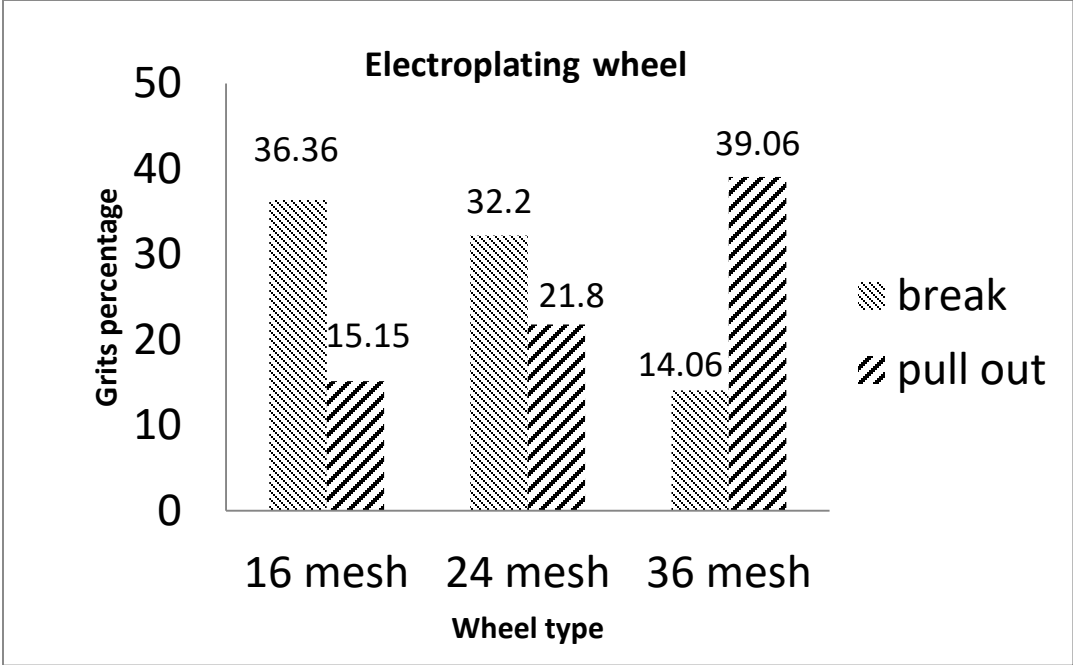


**Fig. 4.24** Percentages of grit pull out and grit breakage for the electroplated wheels

## CHAPTER 5

### Conclusions and Future Scope

#### 5.1 Conclusions

In this study an approach is made to fabricate monolayer grinding wheel by using D-Gun coating technique. Also, the feasibility of using alumina grits to prepare the wheel is studied. By using electroplating, electroless plating and D-Gun coating techniques the monolayer grinding wheel is successfully fabricated. In addition, the performance of the wheel is tested and based on the performance the following conclusions are drawn:-

- Material removal rate (MRR) of the monolayer grinding wheel fabricated by using D-gun coating process is more as compared to the same of conventional wheel. However the life of the monolayer grinding wheel is not long.
- With an increase in grit size the MRR of the wheels increases.
- Number of grits that pulled out of the wheel is less compared to the number of broken grits in case of wheels with Electroplated Ni.
- In case of electroless deposited wheels the grit pullout is more than grit breakage due to the low coating adhesion.
- To increase the life of the wheel in place of  $\text{Al}_2\text{O}_3$  grits super abrasive grits such as diamond or cBN may be chosen. These monolayer wheels can be used for stock removal of substantial amount of material from the work piece and then the conventional wheel may be used to finish the surface.

## 5.2 Future scope

- Coating thickness can be increased to achieve better adhesion between the grits and the wheel-hub.
- Different types of grits such as super-abrasives can be used to increase the life and performance of the wheel.
- Different cutting velocities can be tried to find individual lives of the wheels.
- Effect of depth of cut on wheel lives can also be studied in future.

## References

1. **Marinescu, I.D., Hitchiner, M., Uhlmann, E., Rowe, W. B., Inasaki, I.**, “Handbook of Machining with Grinding Wheels”, **CRC Press**, ISBN- 10: 10: 1-57444-671-1.
2. **Rowe, W. B.**, “Principles of modern grinding technology”, **William Andrew**, ISBN: 978-0-81-552018-4.
3. **Bari, G. A. D., (2010)**, “Electrodeposition of Nickel”, **Modern Electroplating**.
4. **Ding, W. Linke, B. Zhu, Y. Li, Z. Fu, Y. Su, H. Xu, J., (2016)**, “Review on monolayer CBN superabrasive wheels for grinding metallic materials”, **Chinese Journal of electronics**, Vol. 30, Issue 1, 109-134, DOI: 10.1016/j.cja.2016.07.003.
5. **Henry, J.R.**, “Electroless (Autocatalytic) Plating” **Wear-Cote International**,
6. **Davis, J.R.**, “Handbook of Thermal Spray Technology”, **ASM International**, ISBN 0-87170-795-0
7. **Oerlikon**, “An introduction to Thermal Spray”, Issue 6, November 2015, [www.oerlikoon.com](http://www.oerlikoon.com)
8. **Pawlowski, L.**, “The Science and Engineering of Thermal Spray Coatings”, **Praxair Technology**, ISBN 978-0-471-49049-4
9. **Chattopadhyay, A.K., Chollet, L., Hintermann, H.E.**, “Improved monolayer CBN wheel for load free grinding”, **International Journal of Machine Tools and Manufacture**, 32, 1992, 571-581
10. **Chattopadhyay, A.K., Chollet, L., Hintermann, H.E.**, “On Performance of Chemically Bonded Single-Layer CBN Grinding Wheel”, **CIRP Annals**, 39, 1990, 309-312.
11. **Chattopadhyay, A.K., Chollet, L., Hintermann, H.E.**, “On Performance of Brazed Bonded Monolayer Diamond Grinding Wheel”, **CIRP Annals**, 40, 1991, 347-350.

12. **Chattopadhyay, A.K., Hintermann, H.E.,** “On Performance of Brazed Single-Layer CBN Wheel”, **CIRP Annals**, [https://doi.org/10.1016/S0007-8506\(07\)62221-5](https://doi.org/10.1016/S0007-8506(07)62221-5)
13. **Pal, B., Chattopadhyay, A. K., Chattopadhyay, A. B.,** “Development and performance evaluation of monolayer brazed cBN grinding wheel on bearing steel” **International Journal Advance Manufacturing Technology**, DOI 10.1007/s00170-009-2341
14. **Bhaduri, D., Chattopadhyay, A.K.,** “Effect of pulsed DC CFUBM sputtered TiN coating on performance of nickel electroplated monolayer cBN wheel in grinding steel, Surface and Coatings Technology”, **Surface & Coatings Technology**, 204, 2010, 3818-3832.
15. **KeY ,P.L., WuQ , N., Wang ,M.,** “Study on thermal barrier coatings deposited by detonation gun spraying”, **Surface and Coatings Technology**.
16. **Wang, T.G., Liu, Y., Wang, Q., Gong, J., Sun, C., Kim, K.H.,** “Influence of residual stress on the adhesive behavior of detonation gun sprayed”, **Current Applied Physics**, doi:10.1016/j.cap.2012.02.019
17. **Kumar, S., Sriharsha, P., Madhukar, S.,** “Experimental Investigation on Ceramic Surface Coatings on Aluminum using Detonation Gun”, **International journal of current engineering and technology**.